Short-Term Mobility 2017

Relazione scientifica dell'attività
STM2017

Attività di ricerca svolta presso

Istituto dei Sistemi Complessi - sede di Sesto Fiorentino
Consiglio Nazionale delle Ricerche

nel periodo 29 Gennaio-9 Febbraio 2018

Dott. Bruno Tiribilli

Istituto dei Sistemi Complessi del Consiglio Nazionale delle Ricerche ISC-CNR

Italy

Dr. Paolo Paoletti
Senior Lecturer in Control

School of Engineering “The Quadrangle”
The University of Liverpool

United Kingdom

INDICE

1. Il microcantilever come sensore

La risposta dinamica di una levetta di dimensioni micrometriche è influenzata dall'ambiente circostante e, come tale, può essere utilizzata come sensore. In un tipico setup di sensore basato su microcantilever, la sonda viene posta in oscillazione tramite onde acustiche generate da un dither piezo montato vicino alla base. Quando la frequenza della tensione applicata al dither piezo viene variata con continuità, si osserva un aumento dell'ampiezza di oscillazioni intorno alla frequenza corrispondente alla risonanza meccanica della levetta. Il microcantilever può quindi essere utilizzato come sensore monitorando variazioni nella frequenza di risonanza, indotte da cambiamenti nell'ambiente in cui opera la levetta o nella levetta stessa.

In particolare, la collaborazione tra il Dr Tiribilli and il Dr Paoletti si incentra sulla creazione di nuove piattaforme per la misura di massa/concentrazione di molecole in soluzione e per la misura di viscosità di liquidi. In tali piattaforme, la levetta viene posta in auto-oscillazione tramite un circuito di feedback tra la deflessione e l'eccitazione del dither piezo. Come descritto nella relazione STM2016 [1] e pubblicato in [2,3], tale strategia di eccitazione ha permesso di realizzare sensori di viscosità ad alta sensibilità e con rapporto segnale-rumore molto elevato.

2. Descrizione dell'apparato sperimentale

La maggior parte degli esperimenti condotti durante l'attività STM2017 sono stati svolti utilizzando il setup gia' descritto in [1,3]. Tale setup era basato su un microscopio AFM auto-costruito costituito da una meccanica progettata e realizzata dal Dr Tiribilli, un controller programmabile RHK R9 e un circuito di auto-eccitazione progettato e realizzato in collaborazione con Elbatech srl. Gli elementi principali di tale setup sono illustrati in Figura 2.1 e si rimanda a [3] per una descrizione dettagliata di tutti i componenti.

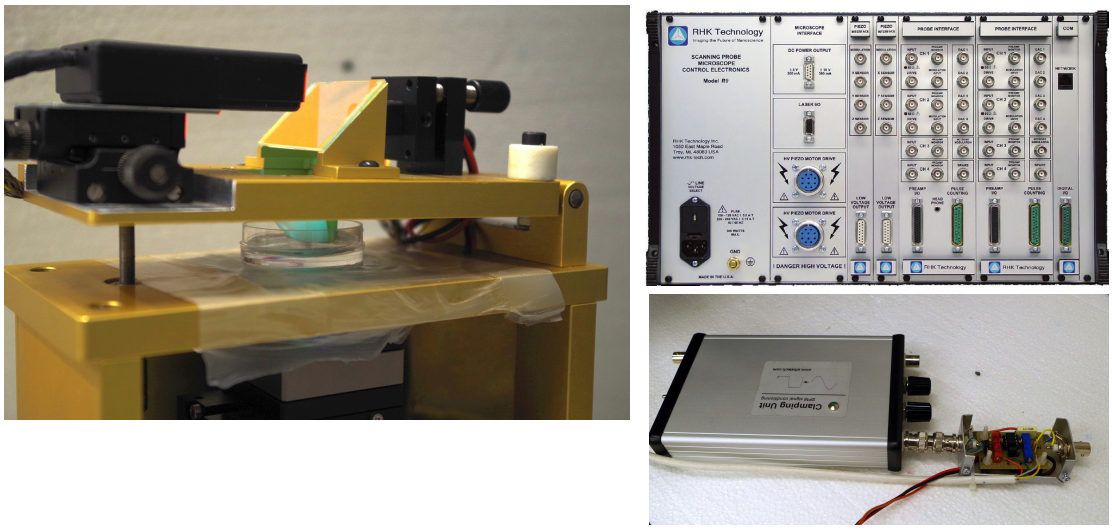

Figura 2.1 – Elementi principali del setup sperimentale utilizzato per l'attività' STM2016 e per misure di massa: (a sinistra) microscopio AFM; (a destra in alto) controller RHK R9; (a destra in basso) circuiti per indurre auto-oscillazioni ed introdurre ritardo.

L'attività STM2016 aveva evidenziato il ruolo fondamentale giocato dal ritardo di fase tra l'eccitazione fornita al dither piezo e la deflessione del cantilever nel determinare il comportamento dinamico della sonda utilizzata come sensore di viscosità o di massa [1]. Purtroppo l'elettronica di auto-eccitazione non permetteva di controllare direttamente il ritardo di fase, ma solo di introdurre un ritardo variabile nell'anello.

Al fine di ovviare a tale limitazione e per comprendere meglio il comportamento del sistema, una nuova elettronica completamente digitale è stata progettata e realizzata in collaborazione con Elbatech srl e FAB crea srl. Uno schema funzionale del circuito è riportato in Figura 2.2.

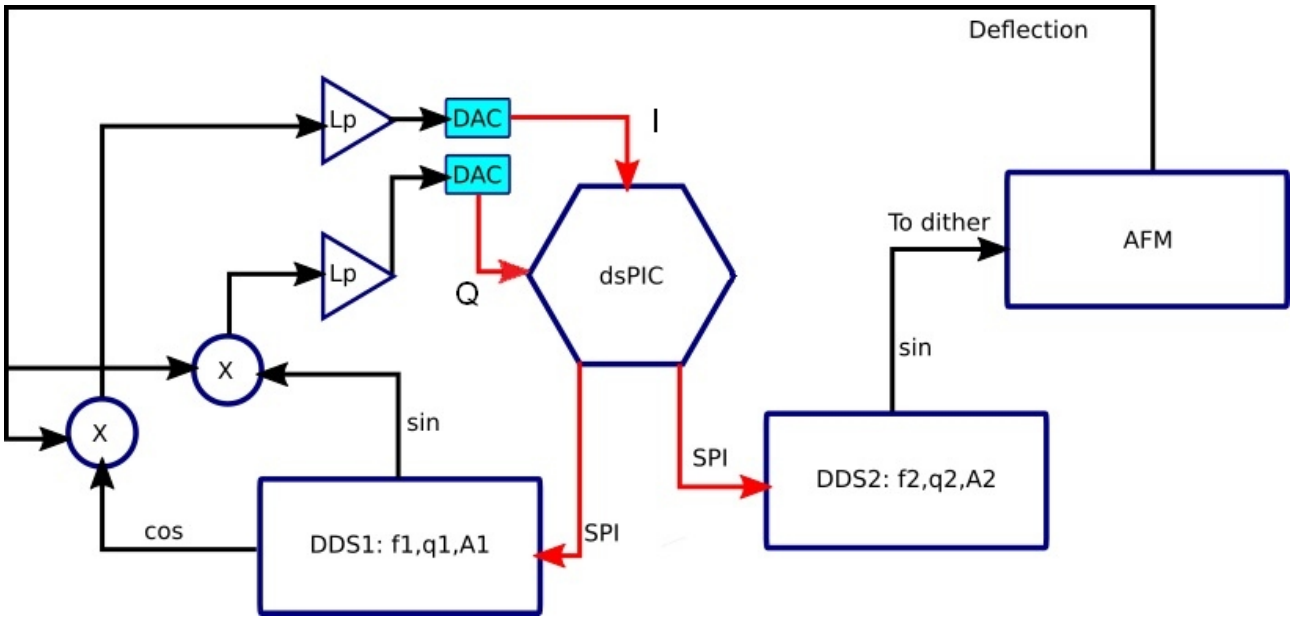

Figura 2.2 – Schema funzionale della nuova elettronica di auto-oscillazione.

Come illustrato in Figura 2.2, il segnale di eccitazione del dither piezo viene generato da un integrato Direct Digital Synthesis (DDS) indicato come DDS2 e controllato da un microcontrollore dsPIC in termini di frequenza e ampiezza. La deflessione delle levetta (rilevata da un fotodiodo a quattro quadranti) viene demodulata grazie ad un secondo DDS indicato come DDS1 nello schema, la cui frequenza viene impostata dal dsPIC in modo da essere uguale a quella del segnale del dither piezo. Le componenti in fase e quadratura vengono quindi filtrate e lette dal dsPIC attraverso due convertitori analogici digitali a 16bit. Infine, il microcontrollore dsPIC comunica con una scheda Raspberry Pi che si occupa della trasmissione dei dati tramite protocollo di rete ad un PC fornito dell'apposito software di controllo. Una foto della scheda fisica testata è riportata in Figura 2.3.

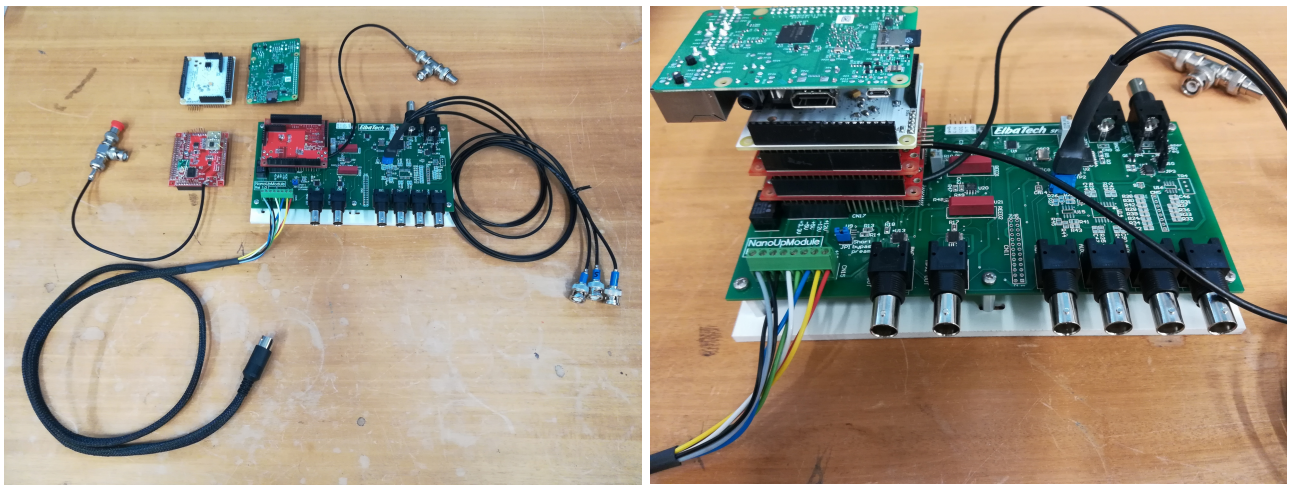

Figura 2.3 – Nuova scheda di auto-eccitazione: componenti (sinistra) e scheda montata (destra).

L'introduzione di oscillatori la cui frequenza, ampiezza e fase possono essere controllati dal dsPIC ha permesso di implementare nel microcontrollore un algoritmo di controllo volto a mantenere la fase tra DDS1 e DDS2 (ovvero tra il segnale di deflessione e quello di eccitazione del dither piezo) ad un valore costante impostabile dall'utente tramite un apposito software di interfaccia. Tale controllo era impossibile da ottenere con la precedente elettronica.

Infine, per controllare meglio l'introduzione di soluzioni acqua-glicerolo nella cella di misura, è stata realizzata una cella apposita fornita di un ingresso da cui introdurre il liquido di interesse e da un'uscita da cui prelevare liquido. Una foto di tale setup è riportata in Figura 2.4.

Figura 2.4 – Setup sperimentale per misure di viscosita': cella di misura con ingressi/uscite per le soluzioni da testare (sinistra) e setup completo (destra). La temperatura di misura e' monitorata tramite una termocoppia montata vicino alla sonda e collegata al termometro da banco visibile sullo sfondo. L'ingresso/uscita delle soluzioni e' regolata attraverso l'uso di siringhe e morsetti per fermare il flusso.

3. Risultati sperimentali

In questa sezione si riporta una selezione dei dati sperimentali acquisiti durante l'attività STM2017. In sezione 3.1 si riportano delle misure di massa ottenute utilizzando la piattaforma già' descritta nella relazione STM2016, in sezione 3.2 viene descritta la caratterizzazione della nuova elettronica e infine nella sezione 3.3 vengono presentate le misure preliminari di viscosità ottenute utilizzando la nuova elettronica.

3.1 - Misure di massa

Al fine di poter testare la possibilità di utilizzare levette in auto-eccitazione per misurare variazioni di massa, sono stati condotti diversi esperimenti (in aria, utilizzando la piattaforma già descitta in STM 2016) in cui si attaccavano sferette di massa nota al cantilever e si andavano a misurare le variazioni di frequenza di oscillazione. Una collezione di immagini di sferette attaccate alla sonda è riportata in Figura 3.1.

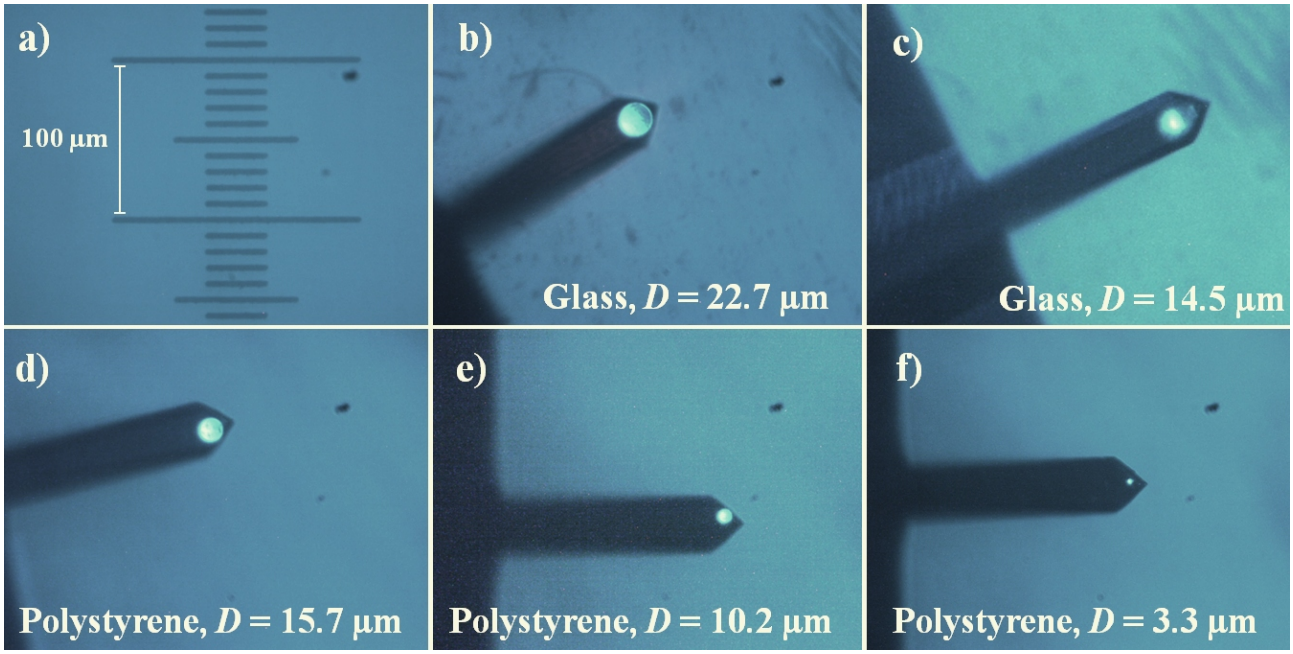

Figura 3.1 – Immagini delle varie sferette di polistirene o vetro attaccate alla levetta per misurare variazioni di frequenza dovute a cambiamenti di massa del cantilever.

Tali misure mostrano che la frequenza di auto-oscillazione diminuisce all'aumentare della massa delle sferette, come atteso. Ulteriori dettagli su questo studio sono riportati nell'articolo "A versatile mass-sensing platform with tuneable nonlinear self-excited microcantilevers" sottomesso dagli autori alla rivista *IEEE Transactions on Nanotechnology* e di cui si riporta il preprint in appendice A

3.2 - Caratterizzazione nuova elettronica

Le prestazioni della nuova elettronica (descritta in sezione 2) sono state caratterizzate tramite due serie di esperimenti: i) andamento e stabilita' della frequenza di auto-oscillazione al variare del ritardo di fase impostato tra l'eccitazione del dither piezo e il

segnale di deflessione; ii) studio del rumore presente nei dati acquisiti dal dsPIC e trasmessi dal Raspberry Pi al PC di controllo.

Per il primo set di esperimenti una levetta di tipo ACST-TL (AppNano, USA) è stata montata sulla testa di misura mostrata in Figura 2.4 e posta in auto-oscillazione in aria utilizzando la nuova elettronica. Il set-point del controller PID responsabile del mantenimento della fase tra eccitazione e deflessione è stato quindi variato tra 0 e 360 gradi a passi di 15 gradi. Come atteso, la variazione della fase comporta una variazione di frequenza e variando la fase è possibile settare a piacere la frequenza di auto-oscillazione intorno al picco di risonanza. Durante tali prove si è evidenziato anche un problema con l'implementazione del controllore PID che veniva resettato tutte le volte che il set-point veniva cambiato, inducendo transitori significativi nel comportamento del sensore. Grazie alla collaborazione con FAB Crea srl è stato possibile cambiare il firmware del dsPIC in modo che tale fenomeno non avvenisse e ciò' è risultato in un miglioramento della stabilita' della misura.

Le prove di caratterizzazione della nuova elettronica hanno anche evidenziato la presenza di un rumore abbastanza elevato nei dati trasmessi al PC di controllo. Tale rumore si manifesta principalmente sotto forma di picchi spuri, come mostrato in Figura 3.2.

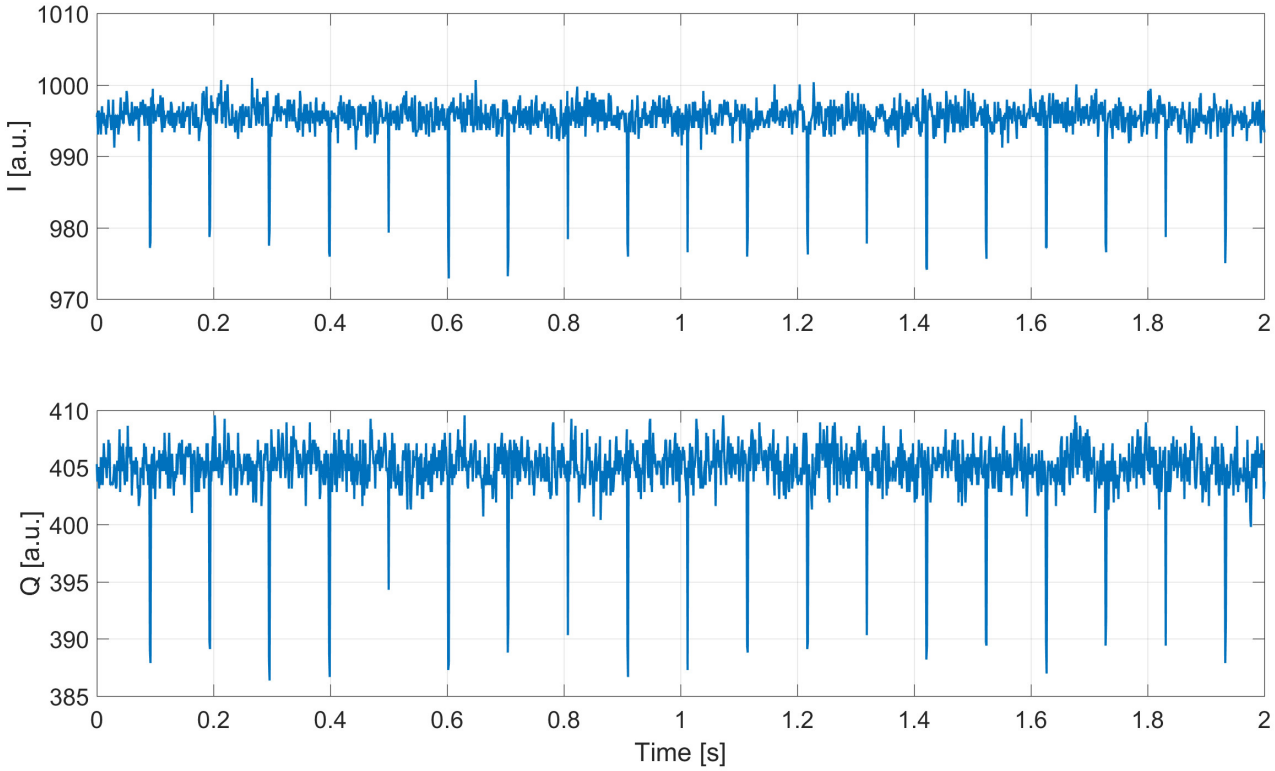

Figura 3.2 –Presenza di rumore e, soprattutto, picchi spuri nei segnali visualizzati e salvati dal software di controllo: componente in fase (in alto) e componente in quadratura (in basso). Ogni unità sull'asse verticale corrisponde a circa 0.25mV

È stata quindi condotta una campagna investigativa volta ad individuare le possibili cause di tali picchi spuri. Tale attività ha permesso di identificare la connessione dsPIC-

Raspberry PI come causa principale di tale fenomeno. La creazione di un nuovo cavo di connessione e la sostituzione di un connettore ha permesso di ridurre l'ampiezza di tali picchi, ma si suggerisce la risaldatura del connettore sulla scheda dsPIC al fine di eliminare tale fenomeno indesiderato.

3.3 - Misure di viscosità con nuova elettronica

Al fine di testare le prestazioni della nuova elettronica in applicazioni di micro-sensoristica, sono stati effettuati diversi esperimenti volti a misurare cambiamenti di viscosità nel fluido in cui la levetta opera. In Figura 3.3 si riporta la serie temporale della variazione di frequenza di auto-oscillazione indotta dall'introduzione di una soluzione acqua-glicerolo (concentrazione glicerolo 5% v/v) e alla successiva rimozione della soluzione tramite immissione di acqua. Dopo il primo riempimento della cella con soluzione di glicerolo (time ~100s) si nota (dati evidenziati in arancione) una variazione di frequenza Δf di circa 260Hz rispetto alla condizione operativa iniziale in acqua (dati indicati in blu). Una seconda immissione di soluzione di glicerolo (time ~ 300s) non altera significativamente la frequenza. Infine una lavaggio (2 passaggi) in acqua ripristina le condizioni iniziali (dati indicati in blu).

Inoltre osservando i transitori (in grigio) si nota come l'immissione di liquido nella cella induca una riduzione della frequenza di auto-oscillazione, mentre la rimozione di liquido comporti un aumento della frequenza. Un'ulteriore indagine sperimentale ha infatti evidenziato come lo spettro di risposta della levetta sia significativamente influenzato dalla quantità di liquido presente nella cella di misura, quindi l'operatore deve porre particolare attenzione al fatto di mantenere costante la quantità di liquido mentre effettua le misure.

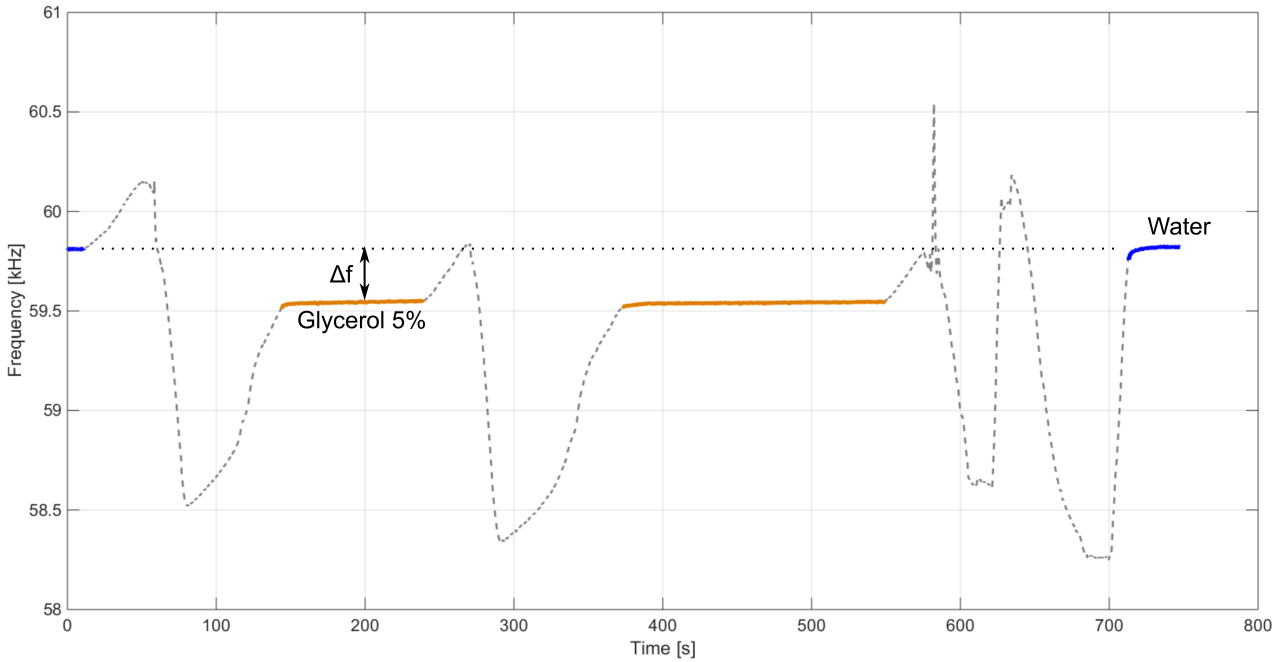

Figura 3.3 – Andamento della frequenza di auto-oscillazione al variare della concentrazione di glicerolo presente nella cella di misura. La variazione Δf della frequenza di auto-oscillazione risulta essere 260Hz tra acqua e soluzione glicerolo al 5% v/v.

4. Nuova piattaforma opto-meccanica

Tutta l'attività condotta finora nella collaborazione tra il Dr Paoletti e il Dr Tiribilli ha utilizzato una piattaforma opto-meccanica derivata da un setup AFM standard. Sebbene l'utilizzo di tale piattaforma abbia permesso di ottenere risultati interessanti, la creazione di uno strumento progettato appositamente per misure di massa e viscosità comporta diversi vantaggi come la drastica riduzione del costo e dell'ingombro (grazie alla rimozione di elementi non più necessari, come la movimentazione del campione). Parte dell'attività STM2017 è stata quindi rivolta alla progettazione e realizzazione di tale piattaforma. Una foto della piattaforma realizzata è riportata in Figura 4.1.

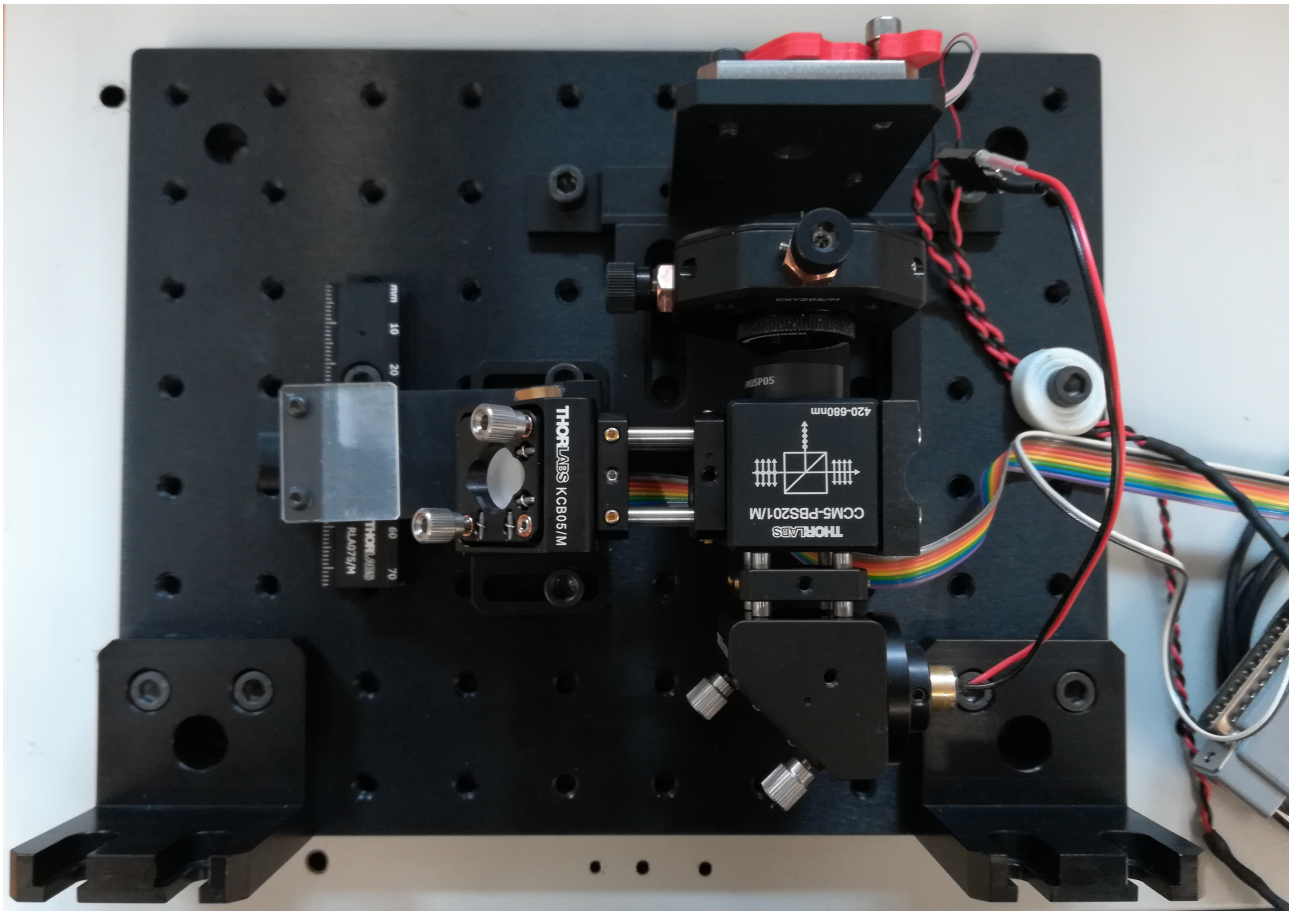

Figura 4.1 – Foto della nuova piattaforma opto-meccanica progettata per misure di massa e viscosità.

La nuova piattaforma è composta da un laser a semiconduttore montato orizzontalmente (in basso a destra in figura) il cui fascio viene immediatamente deflesso di 90 gradi e mandato ad un beam-splitter polarizzatore che lascia passare solo la componente con polarizzazione orizzontale. Il fascio attraversa quindi una lamina a quarto d'onda per creare un fascio a polarizzazione circolare che raggiunge la levetta attraverso un'ottica che permette la focalizzazione e l'allineamento. Una volta riflesso, il fascio torna indietro

fino al beam-splitter che lo deflette di 90 gradi verso un'ottica che indirizza il fascio laser verso un fotodiodo a quattro quadranti al fine di misurare deflessione e torsione del cantilever. In Figura 4.2 si riporta un dettaglio della nuova cella di misura e dello spot laser incidente su un vetrino durante la fase di allineamento, prima di essere deflesso sul fotodiodo a quattro quadranti.

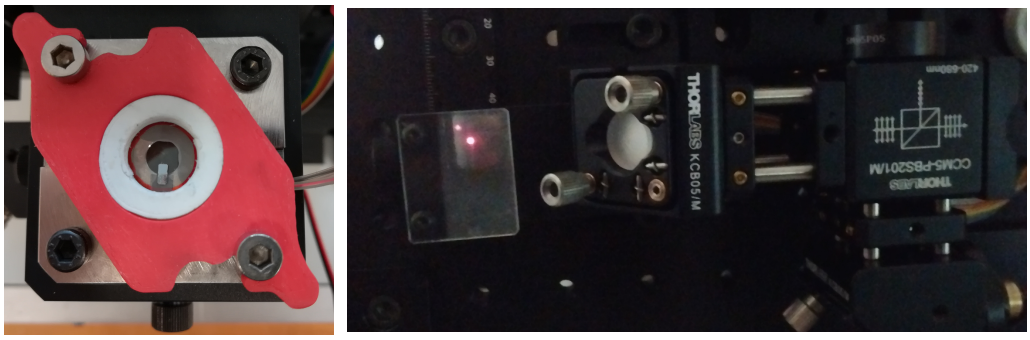

Figura 4.2 – Nuova cella di misura stagna con portalevetta sul fondo (sinistra) e spot laser risultante alla fine del percorso ottico (destra).

Dopo la fase di messa a punto, la nuova piattaforma opto-meccanica è stata testata montando tre levette CLFC-NOCAL (Bruker, UK) aventi frequenze di risonanza diverse A=301,2kHz; B=73,7 kHz; C=18,3 kHz. Come mostrato in Figura 4.3 la piattaforma permette di acquisire spettri di buona qualità.

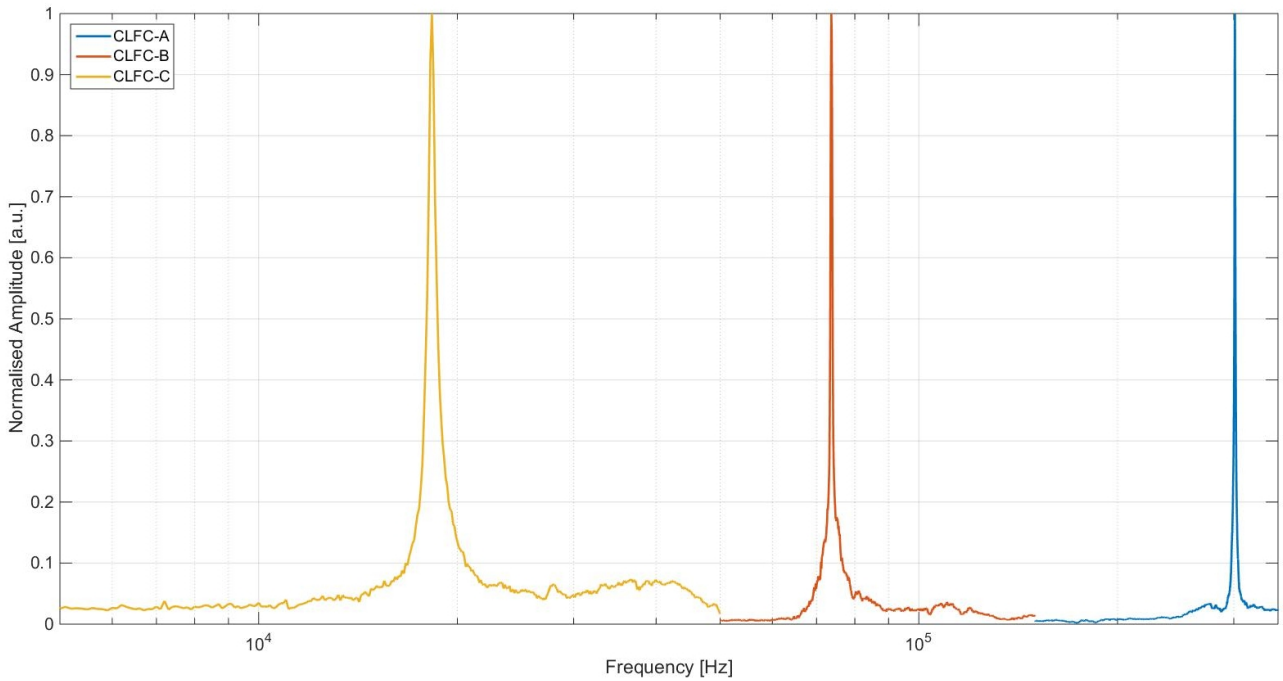

Figura 4.3 – Spettri in frequenza ottenuti con la nuova piattaforma opto-meccanica utilizzando tre levette CLFC (Bruker, UK).

Purtroppo pero’ tali prove hanno evidenziato la presenza di drift e riflessioni spurie sul segnale ricevuto dal fotodiodo a quattro quadranti, quindi un’ulteriore fase di messa a punto deve essere condotta in futuro.

5. Conclusioni e sviluppi futuri

L'attività svolta presso l'Istituto dei Sistemi Complessi ha permesso di testare e caratterizzare una nuova elettronica di auto-oscillazione dotata di controllo automatico dello sfasamento tra deflessione e segnale di eccitazione del dither piezo. Con questa nuova elettronica sono state ottenute misure preliminari di viscosità

Inoltre è stato assemblato la nuova piattaforma opto-meccanica sulla quale sono iniziati i test preliminari che hanno dimostrato la corretta funzionalità di questa configurazione (vedi fig 4.3), sebbene siano state individuate alcune aree che richiedono ulteriore messa a punto come descritto in sezione 4.

Sono state anche individuate le seguenti aree interessanti su cui si propone di continuare la collaborazione:

- Messa a punto e ottimizzazione del nuovo set-up opto-meccanico, in particolare per ridurre drift e riflessioni spurie.
- Progettazione e costruzione di una cella di misura per liquido dotata di accesso ottico.
- Progettazione e costruzione di una cella chiusa di misura per gas collegabile ad un sistema di controllo della pressione.
- Revisione dell’hardware elettronico allo scopo di eliminare i disturbi e minimizzare il rumore.
- Indagine teorica e sperimentale sulla possibilità di ottenere salti di frequenza indotti da variazioni dei parametri ambientali (massa, viscosità) e sulla possibilità di innescare questi salti in regioni di interesse.
- Studio della dinamica della levetta in fluidi non newtoniani e delle componenti elastica, inerziale e dissipativa della interazione fluido-cantilever.

Riferimenti bibliografici

[1] B.Tiribilli and P.Paoletti, Relazione scientifica STM2016

[2] J Mouro, B Tiribilli, P Paoletti “Measuring viscosity with nonlinear self-excited microcantilevers” Applied Physics Letters 111 (14), 144101 (2017)

[3] J Mouro, B Tiribilli, P Paoletti “Nonlinear behaviour of self-excited microcantilevers in viscous fluids” Journal of Micromechanics and Microengineering 27 (9), 095008 (2017)

Appendice A Preprint del paper riguardante misure di massa (attualmente in fase di revisione per pubblicazione nella rivista *IEEE Transactions on Nanotechnology*)

IEEE TRANSACTIONS ON NANOTECHNOLOGY

A versatile mass-sensing platform with tunable nonlinear self-excited microcantilevers

Journal:	*Transactions on Nanotechnology*
Manuscript ID	TNANO-00005-2018
Manuscript Type:	Regular Papers
Date Submitted by the Author:	04-Jan-2018
Complete List of Authors:	Mouro, João; Electrical and Electronic Engineering Tiribilli, Bruno; Istituto dei Sistemi Complessi, Paoletti, Paolo; University of Liverpool, School of Engineering
Keywords:	Nonlinear oscillators, Nanotechnology, Microsensors

A versatile mass-sensing platform with tunable nonlinear self-excited microcantilevers

J. Mouro, B. Tiribilli, and P. Paoletti

***Abstract*—A versatile mass-sensing platform based on the nonlinear dynamical response of microcantilevers embedded in a self-excitation feedback loop is proposed. The dynamical response of the microcantilevers is experimentally studied as a function of the delay introduced in the loop by an adjustable phase shifter and as a function of the mass added to the cantilever. It is shown that, depending on the total delay introduced in the loop, the frequencies and amplitudes of the self-sustained oscillations can vary continuously or abruptly with the mass added to the cantilever, or, alternatively, can be made completely insensitive to this parameter. This behaviour is generic and was registered for a wide range of added masses, suggesting that this platform can be used in three different modalities according to the desired application: i) threshold sensor, where a sudden response is triggered by an arbitrarily small change of added mass; ii) continuous mass sensor, where the oscillation frequency smoothly responds to changes in the added mass to the resonator; and iii) stable microresonator, whose oscillation frequency is independent from the environmental conditions. A complete analytical model to explain the observed experimental results is derived and shows a strong agreement with the measured data.**

***Index Terms*—Mass-sensing, nonlinear oscillations self-excited microcantilever.**

I. Introduction

Microelectromechanical systems (MEMS) have emerged in the last decades as the best candidates for a wide range of technological and scientific applications. Microresonator-based sensors, actuators or signal processing components benefit from the high fundamental resonance frequencies and quality factors (Q) characteristic of these mechanical devices [1]. Their microscopic dimensions and very small active masses render these devices extremely sensitive to external perturbations from the surrounding environment, and were crucial to successfully develop imaging applications [2] or force [3], viscosity [4], temperature [5] and mass sensors [6], [7].

In particular, micromechanical resonators used for mass sensing have the potential to ultimately measure the mass of individual molecules, being only limited by the fundamental noise processes [6]. Typically, the operation of micromechanical mass sensors relies on detecting the resonance frequency shift induced by an additional mass adsorbed on the surface of the probe. The sensitivity is known to be greatly improved by using smaller devices, low-noise motion detection and ultrahigh vacuum. An extreme optimization of these parameters on a single experiment allowed achieving a yoctogram (10^{-24} g) resolution [7]. One of the major concerns that must always be addressed when developing a mass sensor is the reduced bandwidth – often less than 1Hz [8] – due to the large quality factor of externally excited microresonators operating in air, which induces long transients. On the other hand, performing measurements in viscous fluids decreases the quality factors and the sensitivity, and often reveal the presence of the undesired spurious mechanical modes [9], [10]. When measuring the resonance frequency shift caused by the added mass of interest, it is usually assumed that the mass is distributed evenly on the probe surface, which is not necessarily true. In addition, when individual masses, such as cells or proteins, are attached, the response of the resonator depends on the actual position of the added mass [11]. Therefore, negative pressure in hollow cantilevers [12], mechanical traps [13] or centrifugal forces [14] were used to place the particles on a specific position of the resonator.

More recently, strategies where the microresonator is embedded in a feedback loop proved to be very effective in achieving a more selective frequency response, which can be crucial to overcome the low quality factor typically associated with viscous media and the undesired *forest of peaks*. Among the proposed strategies are the Q-control [15], parametric resonance [16], [17] and self-excitation circuits [18], [19]. In addition, using feedback loops makes the response of the resonator faster, which translates to a significant increase of measurement bandwidth. Generally, the resonance frequency of the device is continuously tracked by a frequency-modulated phase-locked loop (PLL), allowing measuring adsorption events in real time with sensitivities in the order of ato- or zeptogram (10^{-18} to 10^{-21} g) [20]-[22]. Applying the same concept for measuring multiple eigenmode frequencies

This work was supported by EPSRC grant no. EP/N026799/1 on Self-Tuning Advanced Rheology Tool, and the CNR Short Term Mobility grants 2015 and 2016.

J. Mouro was with the department of Mechanical, Material and Aerospace Enginnering, University of Liverpool, Brownlow Hill, Liverpool, L69 3GH, United Kingdom. He is now with the Department of Electrical and Electronic Engineering, University of Bristol, Woodland road, Bristol, United Kingdom.

P. Paoletti is with the department of Mechanical, Material and Aerospace Enginnering, University of Liverpool, Brownlow Hill, Liverpool, L69 3GH, United Kingdom

B. Tiribilli is with the Institute for Complex Systems, National Research Council (ISC-CNR), via Madonna del Piano 10, Sesto Fiorentino, Firenze I-50019, Italy

simultaneously allows the determination of position and mass distribution of the analytes [23].

One of the main drawbacks of using feedback loops to improve sensing performance is the presence of different sources of nonlinearities introduced, for example, by the nonlinear electronic components required to process the signals or even by the intrinsic mechanical nonlinearities of the resonator. The analysis of the dynamics of microresonators in presence of mechanical nonlinearities have shown interesting and surprising phenomena, such as stable operation of the resonators far beyond the critical vibration amplitude [24], [25] or bistable regimes [26], [27]. It was also shown that the frequency of oscillation is strongly dependent on the delay affecting the feedback signal [27]-[29].

In this work it is shown how the nonlinear dynamics of a cantilever embedded in a feedback loop composed of a gain, a saturator and a tunable phase-shifter can be used as a high-sensitivity or threshold mass sensor, or as a microresonator whose oscillation frequency can be made independent of the environmental conditions, by controlling its operating conditions. The authors have previously studied and modeled a similar system in [29] and proposed it as a viscosity sensor in [30]. Here, such model is extended to incorporate the presence of the added mass, and the dynamical response of the cantilever is theoretically and experimentally studied as function of the added mass (in the form of attached beads) and of the feedback delay that is introduced in the loop by the phase-shifter.

The paper is organized as follows: in section II the experimental setup is discussed. Special emphasis is given to the description and characterization of the phase-shifter, and to the methods of attaching and measuring the diameters and mass of the beads used to change the mass of the resonator. Experimental results illustrating the nonlinear behavior of the self-excited oscillation frequency for different added masses and delays in the feedback loop are presented in section III. In section IV the nonlinear response of the cantilever is discussed by analyzing the phase condition for the existence of self-sustained oscillations and an analytical model describing the dependence between the loop oscillation frequencies and the added mass is derived. Finally, some conclusions are discussed in section V.

II. EXPERIMENTAL METHODS

A. *Experimental setup*

A schematic of the experimental setup used to study the dynamics of the sensor operating in air is shown in Fig. 1(a). Glass and polystyrene beads are individually attached to the cantilever to simulate attachment of analytes to the probe surface. The cantilever motion is acoustically excited by a dither piezo and optically detected by a four-quadrant detector connected to a R9 controller (RHK Technology). The switch S indicates the possibility of selecting between two different measuring configurations: traditional amplitude modulation (AM mode) or autotapping (AT mode). In AM mode, the dither piezo is externally excited by a function generator, using sinusoidal signals at different frequencies. The amplitude and phase of the deflection signal are measured using a lock-in. Both the function generator and the lock-in are available in the R9 controller itself. In AT mode, the deflection signal coming from the detector is fed into an electronic circuit (Elbatech srl) composed of a tunable phase-shifter, a gain and a saturator, before being fed back to the excitation dither piezo as a voltage to induce self-oscillations of the cantilever. The amplitude and frequency of these oscillations are measured from reading the deflection signal with an external oscilloscope (Tektronix TDS-2022).

The total delay, τ_{tot}, shown in Fig. 1(a) represents the intrinsic delay of the feedback loop, i.e. the time that the deflection signal naturally takes to go around the feedback loop once. This delay is responsible of shifting the initial sinusoidal deflection signal by several periods. It was shown in [29] that the total delay, τ_{tot}, results from individual contributions of the electronic components of the circuit (gain + saturator), τ_{ET}, the electronic elements composing the phase-shifter, τ_{PS}, and the delay caused by the propagation of the elastic waves in the cantilever and holder materials, τ_{CT}. The first two terms, τ_{ET} and τ_{PS}, were individually calculated in [29] by connecting sinusoidal signals to the inputs of these circuits and measuring the phase shift of the corresponding outputs. The last term of the total delay, τ_{CT}, depends on the specific connection between the cantilever and the holder, and must be measured before each experiment.

The adjustable phase-shifter introduced in the feedback loop allows adding an extra phase shift to the natural phase shift induced by the total delay of the system. Its role is to finely control the phase between the cantilever deflection and the dither piezo excitation. Fig. 1(b) shows the electrical schematics of a single stage of the phase-shifter, which works as an all-pass filter capable of shifting the signal by at most -π radians. The complete phase-shifter consists of two of these stages connected in series (inducing a total phase shift of -2π radians), each stage being individually operated by adjusting a potentiometer which controls the value of a resistor, R_i, between 0 and 10.2 kΩ. The values of the capacitances of each stage, C_i, are fixed in the circuit and are chosen accordingly to the working range of frequencies, to guarantee that at least one of the stages can effectively reach the maximum phase shift of -π radians. Finally, there is also the possibility of inverting the polarity of the voltage signal applied to the terminals of the dither piezo, as shown by the parameter p = ±1 of Fig. 1(a). This option allows users to shift the signal by extra -π radians.

To summarize, the two stages of the phase-shifter, combined with the possibility of inverting the polarity of the signal that feeds the piezo, can be used to adjust the phase-shift of the signal along the feedback loop by a complete period (-2π radians). Note that this shift adds to the shift caused by the intrinsic total delay of the system. The influence of feedback delay on the dynamic response of the cantilever with different added masses will be assessed in this work.

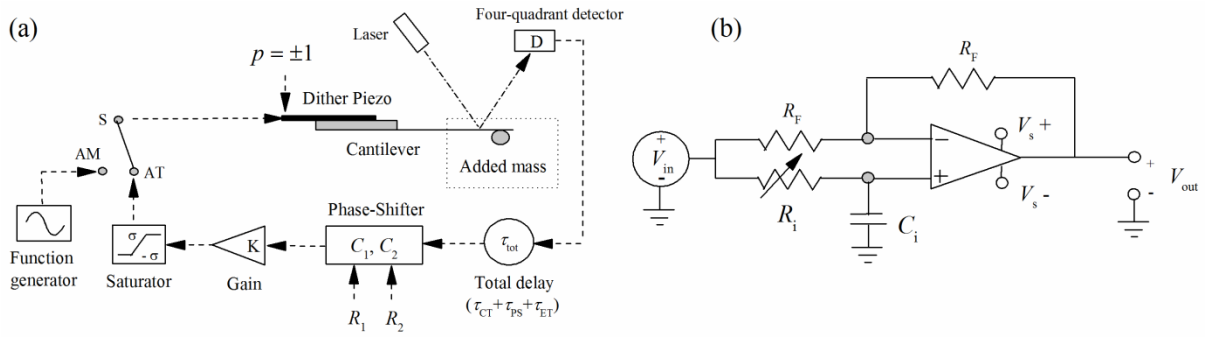

Fig. 1. a) Schematic of the experimental setup. A glass/polystyrene bead is attached to the silicon cantilever. The cantilever motion is acoustically excited by a dither piezo and optically detected using a four-quadrant detector. In amplitude mode (AM), the function generator sweeps the excitation driving frequency, and deflection amplitude and phase are recorded. In autotapping mode (AT), the deflection signal is fed back to the piezo as a voltage, after being shifted by the total delay and by an adjustable phase-shifter, amplified by the gain and limited by the saturator in the feedback loop. The polarity of the voltage applied to the dither piezo can be inverted ($p = \pm 1$). b) Detail of a single stage of the phase-shifter, capable of shifting the signal by at most -π radians. Two stages were connected in series. The values of C_1 and C_2 are 237 pF and 5.14 nF in each stage, respectively, and the two potentiometers R_1 and R_2 are adjustable within the range 0-10.2 kΩ.

The autotapping (AT mode) configuration shown in Fig. 1(a) generates self-sustained stable oscillations of the cantilever with angular frequency ω_{osc}. The onset of the self-oscillations results from a competition between the feedback gain, which constantly amplifies the motion of the cantilever, and the presence of the nonlinear saturation, which constantly limits these trajectories. The system reaches a steady-state and the cantilever self-oscillates with a frequency and amplitude ensuring that the overall loop gain is unitary and that the total phase shift of the signal around the feedback loop is an integer multiple of -2π radians, see section IV [29], [30].

In this work, the dynamic response of the silicon ACST cantilever (from AppNano) vibrating in air with five different beads attached was characterized using the AM and AT configurations. The cantilever natural resonance frequency (in air and with no mass attached) was measured using the AM configuration, while its length and width were estimated from visual inspection on the microscope using the calibrated micrometer ruler shown in Fig. 2(a). Thickness, frequency and spring constant were estimated as described in section II. Table I shows the estimated geometrical and dynamical parameters of the cantilever.

TABLE I
GEOMETRY AND DYNAMICAL PARAMETERS OF ACST CANTILEVER ESTIMATED EXPERIMENTALLY

ACST (AppNano)	Estimated
Length (μm)	160
Width (μm)	33
Thickness (μm) (eq. (1))	2.91
Frequency (kHz)	162.32
Spring Constant (N/m) (eq. (4))	8.92

B. *Attaching the beads*

Different micrometric beads of glass (Monospheres, Whitehouse Scientific LTD) or polystyrene (Latex beads polystyrene, Sigma-Aldrich) were individually attached to the cantilever. The beads were randomly spread on a clean microscope slide and put underneath a home-made AFM setup, in which the position and height of the cantilever connected to its holder can be regulated using two micrometric screws. An optical microscope was placed on top of this apparatus and focused on the beads distributed on the microscope slide. The tipless cantilever was then carefully moved down until its bottom surface went in contact with one single bead. A slight movement of the cantilever was then used to apply a small pressure to the bead and facilitate the attachment. This contact was perceptible on the microscope by the bending of the cantilever. The large ratio between surface and volume of the beads contribute favourably to the attachment of the bead to the cantilever due to surface electrostatic forces. To confirm the attachment, the substrate underneath the cantilever was substituted by a mirrored surface, which allowed observing the bottom side of the cantilever with the bead. Some images, shown in Fig. 2, were recorded with a camera connected to the microscope.

To cover several orders of magnitude of added masses, five beads of different sizes and two different materials were individually attached to the tip of the cantilever: one *small* and one *big* bead of glass, and one *small*, one *medium* and one *big* bead of polystyrene. The diameter of each bead was measured by visual inspection on the microscope and is reported in Table II.

C. *Measuring mass and diameter of the beads*

1) *Optical estimation of bead diameter and mass*

The diameters of the beads were estimated from the images acquired on the microscope. These images were processed using the free software *Gwyddion* [http://gwyddion.net/] and compared with the image of a calibrated micrometric ruler (AmScope MR095 Microscope Stage Calibration Slide). The

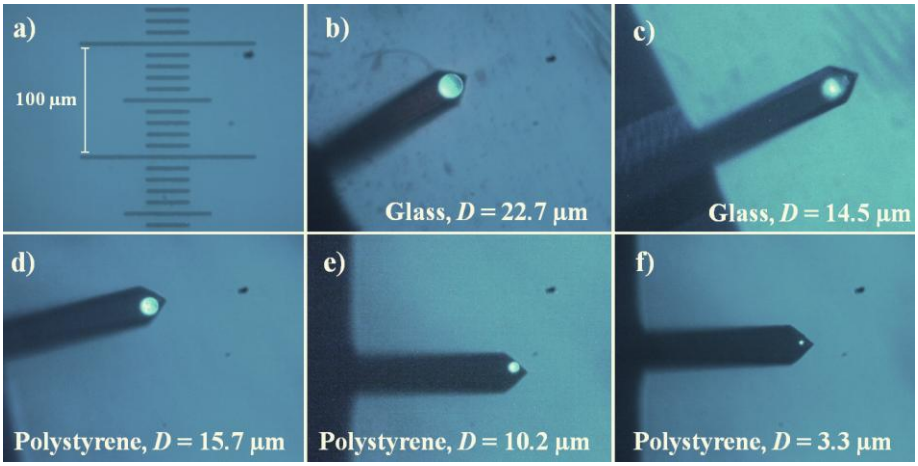

Fig. 2. Optical images of the beads attached to bottom surface of the cantilever and the respective diameters estimated optically. a) Calibration slide used to estimate the dimensions of the cantilever (length and width) and diameter of beads; b) and c) big and small glass beads, respectively; d, e, f) Big, medium and small beads of polystyrene, respectively. All the images have the same magnification.

micrometric ruler and the five beads attached with the respective estimated diameters are shown in Fig. 2.

The mass of the beads was calculated from the optically estimated diameter of each bead, considering the density of the materials [31], [32] and assuming that the beads are perfect spheres. The results are presented in the first two columns of Table II.

2) From the resonance frequency of the cantilever with the beads attached

An alternative way of determining the mass and diameter of each bead is based on the resonance frequency of the cantilever with the beads attached (measured in AM mode). This method allows a more complete characterization of the cantilever, which is useful for the modeling performed in later sections.

The cantilever thickness can be determined from the Euler-Bernoulli beam equation with the appropriate boundary conditions [33], using the value of resonance frequency of the cantilever in air and with no added mass measured in AM mode ($f_0 = \frac{\omega_0}{2\pi} = 162.32\ kHz$) and the estimated length of the beam:

$$T = \omega_0 \frac{L^2}{(1.8751)^2}\sqrt{\frac{12\rho_{CT}}{E}} = 2.91\mu m. \qquad (1)$$

In this equation, $E = 179GPa$ and $\rho_{CT} = 2330kg/m^3$ are the Young's modulus and the density of the silicon, respectively. The calculated value of thickness is reported in Table I.

In this work, the cantilever is modeled as a single-degree-of-freedom damped harmonic oscillator, with an added mass and subject to a hydrodynamic force. This model is an extension of the model presented in reference [30], in which the cantilevers oscillate in viscous fluids. The total hydrodynamic force is described by an inertial and a dissipative term, which account, respectively, for the weight of the layer of fluid that the beam displaces as it moves, and for the viscous drag force exerted by the fluid on the moving cantilever [34]. These two terms can therefore be modeled as a hydrodynamic mass, m_{hydro}, and a hydrodynamic damping coefficient, c_{hydro}, and approximated by [30], [34]-[36]:

$$m_{hydro}(\omega) = \frac{\pi}{4}\rho W^2 L\left(a_1 + \frac{a_2}{W}\sqrt{\frac{2\eta}{\rho\omega}}\right) \qquad (2)$$

$$c_{hydro}(\omega) = \frac{\pi}{4}\rho W^2 L\omega\left(\frac{b_1}{W}\sqrt{\frac{2\eta}{\rho\omega}} + \frac{2\eta}{\rho\omega}\left(\frac{b_2}{W}\right)^2\right). \qquad (3)$$

Both hydrodynamic parameters depend on the angular frequency of oscillation ω, the viscosity η and density ρ of the surrounding fluid, and on the constants a_1 = 1.0553, a_2 = 3.7997 and b_1 = 3.8018 and b_2 = 2.7364. Finally, L and W represent, respectively, the length and width of the cantilever estimated optically and shown in Table I.

According to the harmonic oscillator model, the resonance frequency of the cantilever vibrating in air and with no added mass is given by $\omega_0 = \sqrt{k/m_{r\_0}}$, where k is the spring constant of the cantilever and m_{r_0} accounts for the effective mass concentrated on the tip of the cantilever with no bead attached (the index *0* is used hereafter to denote the case where no bead is attached).

This expression is used to calculate the spring constant of the cantilever, knowing that $f_0 = 162.32\ kHz$ and considering that $m_{r\_0} = 0.24\left(m_{CT} + m_{hydro}(\omega_0)\right)$ [37]:

$$k = {\omega_0}^2\ 0.24\left(m_{CT} + m_{hydro}(\omega_0)\right) = 8.92\ N/m. \qquad (4)$$

In this expression, $m_{CT} = TLW\rho_{CT} = 3.53 \cdot 10^{-11}\ kg$ is the total mass of the cantilever and $m_{hydro}(\omega_0)$ is substituted by the expression given by (2), considering the frequency ω_0 and the properties of the air ($\eta \approx 1.8 \times 10^{-5} Pa\ s$ and $\rho \approx 1.29\ kg/m^3$ [38]). The calculated value of k is presented in Table I. It is worth noting that the value of the spring constant obtained with this method ($k = 8.92\ N/m$) is in close

agreement with the value obtained by the well-known expression $k = \frac{EWT^3}{4L^3} = 8.95\ N/m$ [33].

Finally, the resonance frequency of the cantilever vibrating with the different beads, f_A, (measured in each case using the AM mode) is used to determine the added mass of the beads, m_A, using the expression $\omega_A = \sqrt{k/m_{r\_A}}$, where $m_{r\_A} = 0.24\left(m_{CT} + m_{hydro}(\omega_A)\right) + m_A$ is the effective mass concentrated on the tip of the cantilever (it is assumed that the bead is attached to the tip) [39] and k is the spring constant of the cantilever, calculated from (4) (the index A is hereafter used to denote the presence of an added mass). By rearranging the expression, one obtains:

$$m_A = \frac{k}{{\omega_A}^2} - 0.24\left(m_{CT} + m_{hydro}(\omega_A)\right). \qquad (5)$$

The diameter of each bead can be calculated from its mass, assuming that the bead is a perfect sphere and considering the density of each material [31], [32]. The values of masses and diameters obtained with this method are shown in Table II and show a good agreement with the values obtained from visual inspection.

III. EXPERIMENTAL RESULTS

A. AM Mode – Amplitude and Phase Spectra

Fig. 3 shows a representative example of the experimental amplitude and phase spectra obtained by sweeping the excitation frequency in the AM configuration, for the case of the ACST cantilever with the medium polystyrene bead attached. The measured amplitude spectrum is fitted to the amplitude of the damped harmonic oscillator model, given by the function [8], [40]:

$$A = \frac{H}{\sqrt{\left(\omega_A^2 - \omega^2\right)^2 + \left(\frac{\omega\omega_A}{Q_A}\right)^2}}, \qquad (6)$$

where A is the measured amplitude, ω is the excitation angular frequency of the dither piezo, ω_A is the angular resonance frequency of the cantilever with the added bead (the index A should be substituted by the index 0 in the case of no added mass), Q and H are the quality factors and amplitude of the resonant mode, respectively. The parameters ω_A, Q_A and H were used to fit the model of (6) to the experimental amplitude spectra, as exemplified in Fig. 3(a). The fitted values of resonance frequency, f_A, are used to calculate the mass of each bead using (5) and are shown in Table II, along with the values of Q_A.

Fig. 3(b) shows the phase spectra measured in AM mode, and used to estimate the delay due to the cantilever and its holder, τ_{CT}. This delay is the proportionality constant between the excitation angular frequency ω and the phase shift between the input excitation signal fed to the piezo and the output deflection signal. In AM mode the feedback loop is open and the measured delay just contains information about the mechanical cantilever and holder, excluding the influence of all other electronic components. In fact, τ_{CT} is estimated from the slope of the phase spectrum far from the resonance (to avoid the characteristic jump of -π radians of this region) using:

$$\varphi_{delay} = -\tau_{CT}\omega, \qquad (7)$$

with φ_{delay} in radians, refer to Fig. 3(b). An average delay of $\tau_{CT} \approx 13.9\ \mu s$ was obtained considering the measurements in AM mode of the cantilever with the different beads.

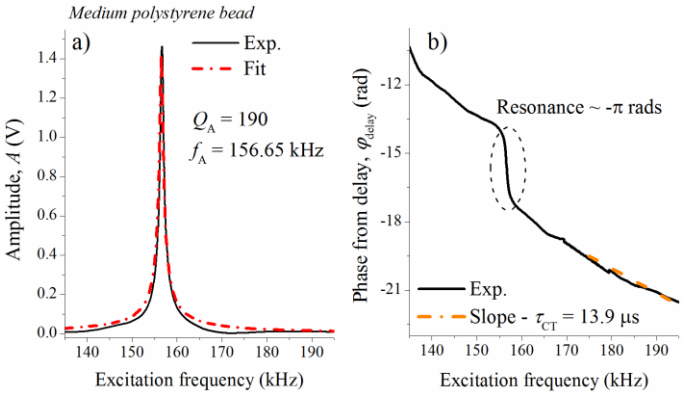

Fig. 3. Experimental amplitude and phase measured in AM mode for the cantilever with the medium- polystyrene bead attached. a) The damped harmonic oscillator model is fitted (red dashed-dotted line) to the measured amplitude (solid black line) and the parameters are extracted; b) The delay on the propagation of the elastic waves through the holder and cantilever materials is extracted from the slope of the phase spectrum away from the resonance. The resonance occurs at 156.65 kHz, as indicated in Table II.

B. AT Mode – Oscillation frequencies as function of signal shift along the loop, for different added masses

Following the characterization in AM mode, the dynamics of cantilever with (or without) the beads operating in the AT configuration was studied as a function of the phase shift, φ_{PS}. The shift of the signal around the feedback loop can be controlled by adjusting the two potentiometers R_1 and R_2 in the phase-shifter shown in Fig. 1 and by inverting the polarity of the signal fed to the dither piezo.

A typical experimental protocol consisted in fixing the value of polarity (p = 1) and the value of R_1, and sweeping the value of R_2 from 0 to 10.2 kΩ. Then the value of R_2 was kept constant while the value of R_1 was swept until reaching 10.2 kΩ. At this stage, the polarity of the piezo was inverted (p = -1) and the potentiometers were sequentially swept back to 0 kΩ. For each set of experimental conditions the frequency and amplitude of the oscillation were recorded.

By sweeping the values of the resistors and inverting the polarity on the piezo the original signal can be shifted by at least a complete period (-2π radians).

Fig. 4 presents examples of experimental results measured using the cantilever with the medium polystyrene bead.

TABLE II
DIAMETERS AND MASSES OF BEADS ATTACHED OBTAINED BY THE TWO PROPOSED METHODS.

	Beads	$D_{bead} \pm 0.5$ (μm) (optically)	m_A (kg) (sphere)	f_A (kHz) (Eq. (6))	Q_A (Eq. (6))	m_A (kg) (Eq. (5))	D_{bead} (μm) (sphere)	% error on D (μm)
No bead	-	-	-	162.32	200	-	-	
Polystyrene (ρ = 1050 kg/ m^3)	*Small*	3.3	1.98e-14	161.15	200	1.83e-14	3.2	3%
	Medium	10.2	5.83e-13	156.65	190	5.25e-13	9.9	3%
	Big	15.7	2.13e-12	145.65	180	1.97e-12	15.3	2.5%
Glass (ρ = 2450 kg/ m^3)	*Small*	14.5	3.91e-12	131.35	130	4.41e-12	15.1	4%
	Big	22.7	1.50e-11	98.27	50	1.47e-11	22.5	1%

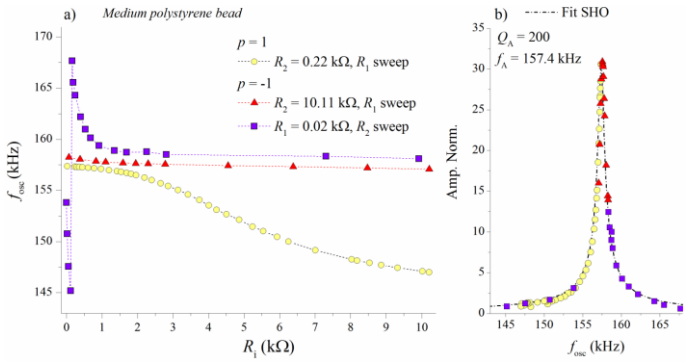

Fig. 4. Frequencies and amplitudes of the self-sustained oscillations, using the medium polystyrene attached to the cantilever. a) Frequencies of oscillation as a function of the values of the resistors in the phase-shifter, for non-inverted or inverted polarity. The dotted lines are guidelines to the eye; b) Amplitude of self-oscillations against the corresponding oscillation frequency for each set of experimental conditions.

Fig. 4(a) shows three series of results obtained when sweeping R_1 or R_2, for two different polarities. Three distinct behaviors, depending on the experimental conditions, can be observed: the series represented by the yellow circles shows a steady decrease on the values of the oscillation frequencies when R_1 increases, for non-inverted polarity. Inverting the polarity, the red triangles show no dependence of the oscillation frequencies with the value of the resistor R_1. Finally, the purple squares show a steep decrease on the values of oscillation frequencies for low values of increasing R_2, before the abrupt jump from low to high frequencies is observed. Then, the steep decrease of oscillation frequencies resume, until a plateau is reached. On the right panel, the amplitude is plotted against the corresponding oscillation frequency, for each set of experimental conditions. It can be observed that this amplitude curve recovers the shape of the amplitude curve measured in the AM configuration (Fig. 3(a)) and it can also be fitted by the harmonic oscillator model with similar parameters.

It is interesting to note in Fig. 4(b) that there are combinations of experimental conditions that induce bigger changes on the oscillation frequencies. These trends are generic and were observed for all cases of different beads.

The best way to compare all the experimental data is to plot the self-sustained oscillation frequencies as a function of the shift caused by the phase-shifter, for each set of experimental conditions and for each bead. This is shown in Fig. 5. The shift induced by the phase-shifter is calculated using (8), explained in detail in section IV, which contains all the experimental parameters (R_1, R_2 and p). The black dashed line represents the case of the cantilever with no added mass and the symbols represent the cases with the different beads attached. It can be observed that the position of the jump moves to more negative values of imposed shift as the added mass increases (the green series with squares, which represents the big glass bead, appears to the right of the initial jump position due to the periodicity of 360 degrees or -2π radians). In addition, the values of oscillation frequency far from the jump correspond to the values of natural resonance frequency of the cantilever with each bead (see Table II). In fact, observing Fig. 4(b) is possible to understand that the measured jumps occur from the high frequency to the low frequency edges of the resonance peak.

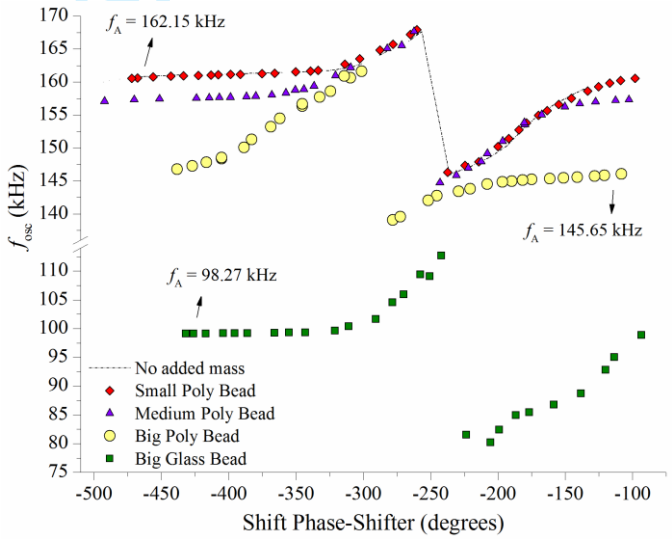

Fig. 5. Cantilever oscillation frequencies plotted against the shift induced by the phase-shifter (calculated with (8)), for each set of experimental conditions. The position of the jump moves to more negative values of imposed shift as the added mass increases. The values of oscillation frequency far from the jump tend to the values of the natural resonance frequency of the cantilever with the added masses. (To improve the clarity of the figure the case of the small glass bead is not shown).

IV. ANALYTICAL MODELING AND INTERPRETATION OF THE EXPERIMENTAL RESULTS

A. Phase of the cantilever vibrating in viscous fluid with an arbitrary added mass

The phase of the cantilever vibrating in a viscous fluid with an arbitrary added mass, m_A, is calculated using the transfer function of the damped harmonic oscillator shown in (6) [30], [39]:

$$\varphi_{CT} = -atan\left(\frac{\omega\gamma}{\omega_A^2-\omega^2}\right) = -atan\left(\frac{\omega(c+c_{hydro})}{k-\omega^2\left(0.24(m_{CT}+m_{hydro})+m_A\right)}\right), \quad (7)$$

where φ_{CT} is the phase of the cantilever, $\gamma = (c + c_{hydro})/(0.24(m_{CT} + m_{hydro}) + m_A)$ is the damping ratio of the cantilever with the added mass m_A, ω is the angular frequency of oscillation and ω_A is the angular resonance frequency of the cantilever with the added mass (the index A should be substituted by the index 0 and $m_A = 0$ in the case of no added mass), and with m_{hydro} and c_{hydro} given by (2) and (3). Finally, k is the spring constant of the cantilever, determined from (4), and $c = \frac{\omega_0 m_{CT}}{Q_0}$ is the intrinsic viscous damping coefficient, obtained from the fit of the damped harmonic oscillator model to the experimental amplitude of the cantilever with no attached mass in AM configuration [30], [39]. When the cantilever vibrates in a viscous medium this parameter is often negligible when compared with c_{hydro}. The dashed-dotted orange curve of Fig. 6 represents the cantilever phase calculated numerically using (7), as function of the oscillation frequency, for the case of no added mass. The geometry of the cantilever shown in Table I and the rheological properties of air [38] were considered in the simulation. The presence of the cantilever will cause a shift in the interval 0 and -π radians between the excitation force and the mechanical deflection.

B. Phase of the elements of the electronic circuit

The elements of the electronic circuit are the gain, the saturator, the total intrinsic delay of the loop and the adjustable phase-shifter. The saturator is the only nonlinear block of the feedback loop. Nevertheless, the output of the nonlinear saturator can be well approximated by a sinusoidal wave having the same frequency as the input, due to the intrinsic band-pass filter characteristics of the resonator embedded in the feedback loop. In other words, the presence of the resonator in the feedback loop attenuates any low frequencies or higher harmonics of the signal caused by nonlinear elements. Therefore, the saturator can be substituted with an amplitude-dependent gain by using the describing function technique [29], [41]. In this case, if the amplitude of the input signal is smaller than the threshold σ (representing the saturation threshold value defined by the user and shown in Fig. 1(a)), the gain is unitary and the output signal is the same as the input. When the amplitude of the input is higher than σ, the output becomes smaller than the input, which contributes to stabilizing the signal that is constantly amplified by the feedback gain. The gain K and the saturator describing function are real functions for each value of amplitude and frequency of the self-sustained oscillation [29], [41]. Therefore, these elements act only on the amplitude of the signal and do not affect its phase.

Conversely, the total delay of the setup introduces a natural shift of the signal given by $\varphi_{tot} = \tau_{tot}\omega_{osc}$, with φ_{tot} in radians, where ω_{osc} is the angular oscillation frequency. The delay τ_{tot} is the sum of three distinct contributions, see section II. The first two terms were measured in [29], where this electronic circuit was used for the first time ($\tau_{PS} = 1.0\ \mu s$ and $\tau_{ET} = 1.1\ \mu s$), and the delay introduced in the loop by the cantilever and holder, τ_{CT}, was measured in section III from the phase curve in the AM configuration ($\tau_{CT} = 13.9\ \mu s$). Therefore, $\tau_{tot} = \tau_{PS} + \tau_{ET} + \tau_{CT} = 16.0\ \mu s$. The dotted green line in Fig. 6 represents the total delay of the system plotted against the oscillation frequency.

The complete transfer function of the phase-shifter is given by $PS(j\omega) = pH_1(j\omega_{osc})H_2(j\omega_{osc})$, where $H_i(j\omega_{osc}) = \frac{1-j\omega_{osc}R_iC_i}{1+j\omega_{osc}R_iC_i}$ is the transfer function of each stage. The phase-shifter causes a total shift of the signal

$$\varphi_{PS} = \pi P - 2\,atan(\omega_{osc}R_1C_1) - 2\,atan(\omega_{osc}R_2C_2), \quad (8)$$

with φ_{PS} in radians, and using the parameter P to model the inversion of polarity in the dither piezo (for convention, p = 1 and P = 0 for non-inverted polarity and p = -1 and P = -1 for inverted polarity). In this work, $C_1 = 237\ pF$ and $C_2 = 5.14\ nF$. Examples of the shift created by one stage of the phase-shifter with inverted polarity are shown in blue in Fig. 6.

Finally, the total shift of the signal imposed by the electronic circuit, φ_{elec}, for fixed experimental conditions results from contributions of all the elements and reads:

$$\varphi_{elec} = \pi P - 2\,atan(\omega_{osc}R_1C_1) - 2\,atan(\omega_{osc}R_2C_2) - \omega_{osc}\tau_{tot}. \quad (9)$$

C. Phase condition for the existence of self-sustained oscillations

The existence of self-sustained oscillations in the feedback loop implies that the deflection signal repeats itself after a complete loop in the self-excitation scheme. Formally, this condition can be stated as [28], [29]:

$$y(t) = K\psi(a)pCT(j\omega)PS(j\omega)e^{-j\omega\tau_{tot}}y(t)$$
$$\Rightarrow K\psi(a)pCT(j\omega)PS(j\omega)e^{-j\omega\tau_{tot}} = 1, \quad (10)$$

where $y(t)$ represent the probe deflection, $CT(j\omega)$, $PS(j\omega)$ and $e^{-j\omega\tau_{tot}}$ are the transfer functions of the cantilever, phase-shifter and total delay of the setup, respectively, the parameter $p = \pm 1$ accounts for the polarity applied on the terminals of the dither piezo, K represent the gain and $\psi(a)$ the describing function of the saturator used in the experimental feedback

loop, with a being the amplitude of the saturator input. Given that the gain K and the describing function of the saturator $\psi(a)$ [41] are real functions and do not affect the phase of the signal, (10) can be decomposed into its real and imaginary parts:

$$K\psi(a)Re[G(j\omega)] = 1, \quad (11)$$

$$Im[G(j\omega)] = 0, \quad (12)$$

where $G(j\omega) = pCT(j\omega)PS(j\omega)e^{-j\omega\tau_{tot}}$. Equation (11) shows that the overall loop gain must be unitary, while (12) states that the total phase shift around the loop must be an integer multiple of 2π radians. By decomposing the total phase of the transfer function $G(j\omega)$ and using (9), equation (12) can be rewritten as:

$$\varphi_{CT} + \varphi_{elec} = 0 \ (mod\ 2\pi). \quad (13)$$

where φ_{CT} is the phase of the cantilever oscillating at ω_{osc}. Equation (13) describes the phase condition for the existence of self-sustained oscillations. It shows that the cantilever will adjust its phase (and hence its oscillation frequency, ω_{osc}) in order to compensate the total phase, φ_{elec}, imposed by the phase-shifter (function of R_1, R_2 and ω_{osc}), the polarity on the piezo (function of P) and the total intrinsic delay of the system (function of ω_{osc} and τ_{tot}).

Fig. 6 illustrates how (13) can be used to explain the observed experimental results shown in section III. This figure shows the phase associated with each element of the circuit plotted against the oscillation frequency. The overall phase is then calculated by adding all the terms together. The values of frequency for which the overall phase matches a multiple of -2π radians are the solutions of (13). These solutions are represented by the black circles on top of the dashed-dotted red horizontal lines.

Fig. 6 illustrates the effect of systematically increasing the values of the resistor R_1, as shown in Fig. 4(a) (only the first stage of the phase-shifter is considered with inverted polarity, $P = -1$). It can be observed that for a small value of R_1 ($R_1 = 2k\Omega$, dotted line) the oscillation frequency solving (13) is given by $f_{osc} = 150\ kHz$, corresponding to a total phase shift of -6π radians. This frequency is lower than the natural resonance frequency of the cantilever with no added mass ($f_0 = 162.32\ kHz$). An increment of R_1 increases the shift introduced by the phase-shifter in the system. Therefore, the oscillation frequency is forced to decrease, and the magnitudes of the phase shifts introduced by the cantilever and total delay decrease as well to keep the sum constant. When this compensation is no longer possible (case of $R_1 = 4\ k\Omega$, dashed-dotted line) the system jumps to the solution -8π radians with an $f_{osc} = 180\ kHz$. After this point, the shifts to lower frequencies resume (case of $R_1 = 8\ k\Omega$, solid line, $f_{osc} = 170\ kHz$), to compensate for the larger shift introduced by the phase-shifter. This process describes the shifts and jumps experimentally observed and plotted in Fig. 4.

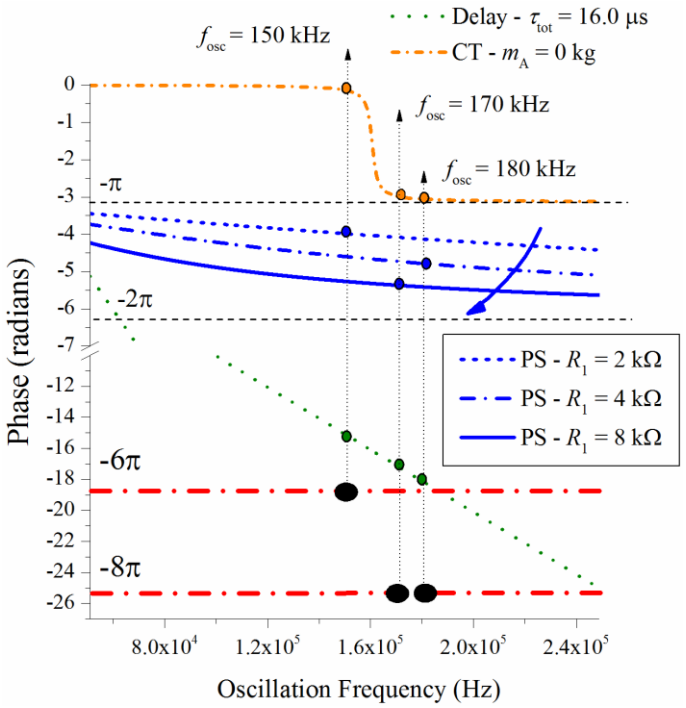

Fig. 6. Interpretation of the experimental results presented in section III using the phase condition for the existence of self-sustained oscillations. Effect of changing the phase introduced by the phase-shifter (by changing R_1), for constant cantilever phase, total delay and polarity.

D. Self-sustained oscillation frequency as function of added mass

Equation (13) allows to calculate the phase of the cantilever for each set of experimental conditions (R_1, R_2, p) and for a self-sustained oscillation with frequency ω_{osc}. Nevertheless, a systematic way of finding which multiple of -2π radians solves such phase condition is required. This task can be algorithmically performed by imposing the physical constraint that the cantilever phase must be in the range $-\pi < \varphi_{CT} < 0$, in agreement with the simple harmonic oscillator model. If the generic value φ_{elec} is written in the form $\varphi_{elec} = a - n\pi$, with $0 < a < \pi$ and $n = 1, 2, 3, \cdots$, the value of the cantilever phase is simply given by $\varphi_{CT} = -a$. Table III illustrates this procedure for some intervals of values of φ_{elec}, with specific examples.

By imposing that the phase $\varphi_{CT} = -a$ of the cantilever oscillating in closed-loop at frequency ω_{osc} is the same as the phase of the cantilever modelled as a damped harmonic oscillator in (7), one obtains:

$$\left(\frac{\omega_{osc}(c+c_{hydro})}{k-\omega_{osc}{}^2\,(0.24(m_{CT}+m_{hydro})+m_A)}\right) = -x \quad (14)$$

with $x = tan(\varphi_{CT})$, and $\varphi_{CT} = -a$, calculated using the algorithm shown in Table III. Equation (14) can be rearranged in order to obtain an explicit dependence between the added mass, m_A, and the self-sustained oscillation frequency, ω_{osc}:

$$m_A = \frac{(c+c_{hydro})}{\omega_{osc}\,x} + \frac{k}{(\omega_{osc})^2} - 0.24(m_{CT} + m_{hydro}). \quad (15)$$

TABLE III

PHASE OF CANTILEVER, φ_{CT}, WORKING IN CLOSED-LOOP AS FUNCTION OF φ_{elec}

φ_{elec} (radians)		$\varphi_{elec} = a - n\pi$ $0 < a < \pi$ and $n = 1, 2, 3, \cdots,$		$\varphi_{CT} = -a$ (radians)
$[0, -\pi]$	$\varphi_{elec} = -1.0$ $\varphi_{elec} = -2.5$	$\varphi_{elec} = a - \pi$	$\varphi_{elec} = 2.14 - \pi$ $\varphi_{elec} = 0.64 - \pi$	$\varphi_{CT} = -2.14$ $\varphi_{CT} = -0.64$
$[-\pi, -2\pi]$	$\varphi_{elec} = -3.5$ $\varphi_{elec} = -6.0$	$\varphi_{elec} = a - 2\pi$	$\varphi_{elec} = 2.78 - 2\pi$ $\varphi_{elec} = 0.28 - 2\pi$	$\varphi_{CT} = -2.78$ $\varphi_{CT} = -0.28$
$[-2\pi, -3\pi]$	$\varphi_{elec} = -7.0$ $\varphi_{elec} = -8.5$	$\varphi_{elec} = a - 3\pi$	$\varphi_{elec} = 2.42 - 3\pi$ $\varphi_{elec} = 0.92 - 3\pi$	$\varphi_{CT} = -2.42$ $\varphi_{CT} = -0.92$

Finally, the expressions for the hydrodynamics mass and damping coefficient, (2) and (3), can be introduced in (15) and an analytical expression relating the oscillation frequency of the cantilever vibrating in the feedback loop immersed in a viscous fluid and with a generic added mass is obtained:

$$m_A = \frac{1}{f_{osc}\, x}\left(\frac{c}{2\pi} + \frac{Lb_2\eta}{4}\right) + \frac{WL}{4}\sqrt{\frac{\rho\eta\pi}{f_{osc}}}\left(\frac{b_1}{x} - 0.24a_2\right) + \frac{k}{(2\pi f_{osc})^2} - 0.24\left(\frac{\pi}{4}\rho W^2 L a_1 - m_{CT}\right). \quad (16)$$

The intrinsic damping coefficient, c, is assumed constant for all range of added masses, which is an approximation (see the decrease of the quality factors, Q_A, with the increase in added mass in Table II). Nevertheless, while vibrating in air, the quality factors are high enough for this approximation to be reasonable. On the other hand, when the cantilever is immersed in a viscous fluid, c is negligible when compared with c_{hydro}.

According to the model developed here, (16) is a necessary condition for the existence of self-sustained oscillations in the feedback loop, but it does not provide any information on the stability of these solutions. This fact becomes relevant due to the presence of the periodic parameter $x = tan(\varphi_{CT})$ in (16). In this case, different values of oscillation frequencies f_{osc} will satisfy (16) for the same value of added mass m_A. The Nyquist Stability Criterion [41] can be used as a secondary criterion to assess the stability of the solutions: it states that the only stable solution of the system is the one with the highest real part of the transfer function $G(j\omega) = pCT(j\omega)PS(j\omega)e^{-j\omega\tau_{tot}}$ (refer to [29, 30] for examples where this criterion has been successfully exploited to understand the stability of viscosity sensors).

Equation (16) and the transfer function $G(j\omega)$ are plotted in Fig. 7 considering a constant value of $R_1 = 0.02\ k\Omega$, but a range of different values for R_2 and the two different polarities. For comparison, the dependence between the resonance frequency and the added mass of the same cantilever working in the traditional AM mode, given by (5), is also plotted in Fig. 7. The geometrical and dynamical parameters of the cantilever are reported in Table I and the rheological parameters of the air [38] were used in the models.

In general, it can be observed that the oscillation frequencies decrease with the increase of the added mass, for the three different curves ($R_2 = 10.12\ k\Omega$, $R_2 = 0.32\ k\Omega$ and $R_2 = 0.02\ k\Omega$, respectively green, orange and purple lines). In addition, the solutions of (16) are shown to be periodic, with branches of solutions for different ranges of oscillation frequencies. The sudden jumps of the oscillation frequencies observed experimentally correspond to a change of the solution branch, for a particular set of conditions. As explained, the real part of the transfer function $G(j\omega)$ is shown as an inset of the figure, to decide the stability of each solution branch. The values of oscillation frequencies measured experimentally using the same conditions than those used to plot (16) are presented in Table IV. This experimental data is added to Fig. 7 as colored circles and show a very good agreement with the respective modeled results.

Fig. 7(a) shows the case of non-inverted polarity ($p = 1$). In this case, the solution of (16) is univocal for small added masses and there are no possibilities for jumps. Then, for an added mass of $m_A \sim 2.0 \times 10^{-12}$ kg a second branch of solutions appears at lower frequencies. A possible jump is illustrated for $m_A \sim 4.0 \times 10^{-12}$ kg (purple squares on top of the purple line of $R_2 = 10.12\ k\Omega$). In this case, the real part of the transfer function $G(j\omega)$ becomes larger for the solution at $f_{osc} = 124\ kHz$ than the solution at $f_{osc} = 158\ kHz$, and the former becomes the stable branch.

Fig. 7(b) shows the case of inverted polarity ($p = -1$). The first thing that can be noted is that the solutions of oscillation frequencies are complementary to those shown in Fig. 7(a). In this case, the modeled operation conditions allow the occurrence of a jump at very small added masses ($m_A \sim 2.0 \times 10^{-14}$ kg). This is the jump observed experimentally in Fig. 5 for the case of the small polystyrene bead (red circles). In addition, the jump shown in Fig. 5 for the case of the big glass bead (green squares) is also presented, for $m_A \sim 1.5 \times 10^{-11}$ kg. Both jumps are indicated by the orange squares.

Fig. 7 shows that the results predicted by the proposed analytical model are in close agreement with the experimental measurements and that the model describes each aspect of the dynamical response of the system observed in Figs. 4 and 5. A deeper analysis of the model and data presented in this figure suggests the possibility of using this platform in three distinct ways, by adjusting the behavior of the sensor via R_1, R_2 and p. The first possibility is to use this device as a continuous mass sensor, whose oscillation frequency depends on the added mass to the cantilever.

TABLE IV

EXPERIMENTAL DATA PLOTTED IN FIG. 7 AS COLORED CIRCLES

$R_1 = 0.02$ kΩ R_2 (kΩ)		*No mass*	*Small Poly* ~ 2 x 10^{-14} kg	*Medium Poly* ~ 5 x 10^{-13} kg	*Big Poly* ~ 2 x 10^{-12} kg	*Big Glass* ~ 1.5 x 10^{-11} kg
$p = 1$	0.02	-	-	154.82 kHz	-	-
	0.32	159.33 kHz	160.56 kHz	-	146.23 kHz	-
	10.12	-	-	-	-	85.19 kHz
$p = -1$	0.02	-	150.59 kHz	-	-	-
	0.32	166.98 kHz	-	165.09 kHz	139.57 kHz	-
	10.12	-	-	158.3 kHz	-	99.23 kHz

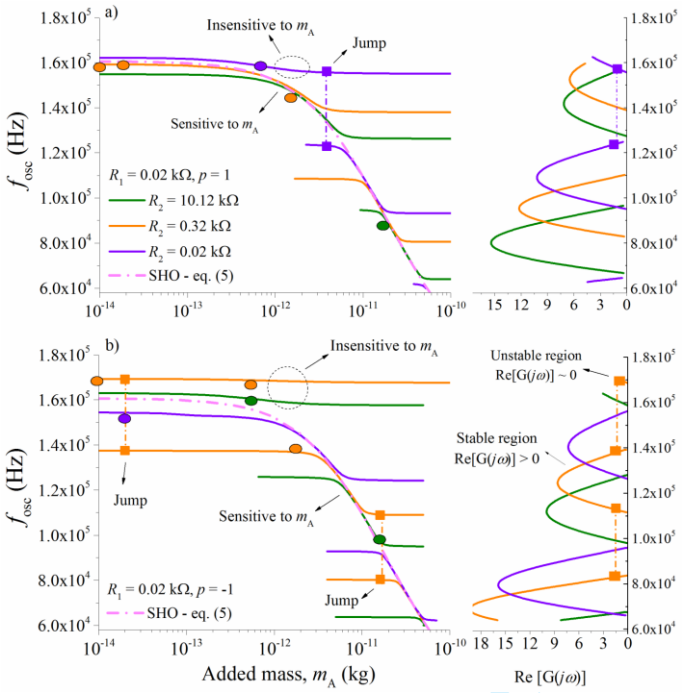

Fig. 7. Predictions of (16), showing the self-sustained oscillation frequencies as function of the mass added to the cantilever. Predictions from a simple externally excited harmonic oscillator given by (5) are shown with dashed lines, for comparison. a) Non-inverted polarity, p = 1; b) Inverted polarity, p = -1. Insets on the right panel: real part of the transfer function $G(j\omega) = pCT(j\omega)PS(j\omega)e^{-j\omega\tau_{tot}}$, used to identify the stable solution according to the Nyquist Stability Criterion. The coloured circles indicate the respective experimental measurements (Table IV), while the squares indicate possible jumps. Three potential working modalities (continuous sensor, threshold sensor and stable resonator) are illustrated.

It is shown that, by playing with the operating conditions, the response of this sensor follows the response of the microresonator working in open-loop (given by the dashed-dotted magenta line representing (5)). Thus, the ultimate sensitivity of the sensor working in closed-loop is the same as the microresonator working in open-loop, but with better signal-to-noise ratio and resolution, typical of the closed-loop setups. In the case of this work, added masses of the order of 10^{-14} kg (small polystyrene bead) were easily detected with a shift in frequency of around 150 Hz. Note that such added mass is well within the "flat" region of the AM mode, where small resonance frequency variations are difficult to detect due to the poor signal-to-noise ratio. The second possibility is to use this platform as a threshold sensor, in which a small variation of mass causes a sudden jump on the oscillation frequencies. Furthermore, it is shown that the location of the abrupt jump can be positioned in the range of added masses of interest by controlling the operating conditions, and in particular by tuning the potentiometers R_1 and R_2 in the phase shifter. Finally, the third possible way of operating this platform is as a stable microresonator, whose oscillation frequency is basically independent of the added mass. Fig. 7 shows regions where the oscillation frequency of the resonator completely deviates from the response characteristic of the open-loop, and is almost constant for a wide range of added masses. A resonator insensitive to environmental conditions can be used for applications where, for example, a stable signal is required for precision timing and frequency references [42]. In reference [30] it was shown that, for specific operation conditions of this platform, the microresonator can also be insensitive to the viscosity of the medium. Such a device could be used to decouple the effect of simultaneous external factors acting on the resonator, for example a chemical reaction where the added mass to the cantilever and the viscosity of the medium change simultaneously [43].

V. CONCLUSIONS

The dynamical response of a microcantilever self-oscillating in a feedback loop is experimentally studied as a function of the mass added to the cantilever and as a function of the phase shift of the signal along the loop. An analytical model capable of explaining the observed phenomena is proposed by describing the microcantilever as a variable mass harmonic oscillator immersed in a viscous fluid and by exploiting a phase condition for the existence of self-sustained oscillations. The experimental and modeled results suggest that this platform can be used in three distinct modes, according to the chosen operation conditions. The first working mode is continuous mass sensing. In this case, the oscillation frequency changes smoothly with the mass added to the cantilever, in a similar fashion and with the same ultimate sensitivity as the cantilever working in traditional AM mode. Nevertheless, the closed-loop scheme allows obtaining a better resolution and signal-to-noise ratio than the traditional open-loop technique. The second working mode is threshold mass sensing. In this case, an arbitrarily small added mass can induce a sudden jump on the oscillation frequency. Furthermore, the location of the abrupt jump can be positioned in the range of added masses of interest by controlling the phase of the cantilever with the adjustable phase-shifter. This feature can be extremely useful in applications such as point-of-care diagnosis, where the presence of an analyte of interest above a certain concentration must be assessed. Finally, this platform can also work as a stable microresonator, whose oscillation frequency is independent of some environmental condition (added mass, viscosity or density). This feature can prove to be extremely important in applications where a stable resonance frequency, independent of the external factors, is required, or to decouple the effect of competing external parameters on the dynamical response of the resonator. These degrees of flexibility are not available with current microcantilever-based mass sensors.

ACKNOWLEDGMENT

The authors wish to thank Elbatech srl for the support in the design and realization of the self-excitation electronics. The data presented in this paper are freely available at https://doi.org/10.5281/zenodo.1095581

REFERENCES

[1] K. L. Ekinci and M. L. Roukes, "Nanoelectromechanical systems", *Review of Scientific Instruments* vol. 76, pp. 061101-1-061101-12, 2005.

[2] L. Manning, B. Rogers, M. Jones, J. D. Adams, J. L. Fuste and S. C. Minne, "Self-oscillating tapping mode atomic force microscopy, *Review of Scientific Instruments*, vol. 74 no. 9, pp. 4220-4222, 2003.

[3] J. Moser, J. Güttinger, A. Eichler, M. J. Esplandiu, D. E. Liu, M. I. Dykman and A. Bachtold, "Ultrasensitive force detection with a nanotube mechanical resonator", *Nature Nanotechnology*, vol. 8, pp. 493-496, 2013.

[4] N. Belminoud, I. Dufour, A. Colin and L. Nicu, "Rheological behaviour probed by vibrating microcantilevers", *Applied Physics Letters*, vol. 92, pp. 041907-1-041907-3, 2008

[5] X. C. Zhang, E. B. Myers, J. E. Sader and M. L. Roukes, "Nanomechanical torsional resonators for frequency-shift infrared thermal sensing", *Nanoletters*, vol. 13, no. 4, pp. 1528-1534, 2013.

[6] K. L. Ekinci, W. T. Yang and M. L. Roukes, "Ultimate limits to inertial mass sensing based upon nanoelectromechanical systems", *Applied Physics Letters*, vol. 95, no. 5, pp. 2682-2689, 2004.

[7] J. Chaste, A. Eichler, J. Moser, G. Ceballos, R. Rurali and A. Bachtold, "A nanomechanical mass sensor with yoctogram resolution", *Nature Nanotechnology*, vol. 7, pp. 301-304, 2012.

[8] T. R. Albrecht, P. Grutter, D. Horne and D. Rugar, "Frequency modulation detection using high-Q cantilevers for enhanced force microscope sensitivity", *J. Appl. Phys.* vol. 69, no.2, pp. 668-673, 1991.

[9] J. Tamayo, M. Alvarez and L. M. Lechuga, "Digital tuning of the quality factor of micromechanical resonant biological detectors", *Sensors and Actuators B*, vol. 89, pp. 33-39, 2003.

[10] B. Gotsmann and H. Fuchs, "Dynamic AFM using the FM technique with constant excitation amplitude", *Applied Surface Science* vol. 188, no. 3, pp. 355–362, 2002.

[11] S. Dohn, S. Schmid, F. Amiot and A. Boisen, "Position and mass determination of multiple particles using cantilever based mass sensors", *Applied Physics Letter*, vol. 97, pp. 044103-1-044103-3, 2010.

[12] D. Ossola, P. Dorig, J. Voros, T. Zambelli and M. Vassalli, "Serial weighting of micro-objects with resonant microchanneled cantilevers", *Nanotechnology*, vol. 27, pp. 415502-1-415502-10, 2016.

[13] J. Lee, W. Shen, K. Payer, T. P. Burg and S. R. Manalis, "Toward attogram mass measurements in solution with suspended nanochannel resonators", *Nano Letters*, vol. 10, no. 7, pp. 2537-2542, 2010.

[14] Y. Weng, F. F. Delgado, S. Son, T. Burg, S. C. Wasserman and S. R. Manalis, "Mass sensors with mechanical traps for weighing single cells in different fluids", *Lab on a Chip*, vol. 11, pp. 4174-4180, 2011.

[15] T. R. Rodríguez and R. García, "Theory of Q control in atomic force microscopy", *Applied Physics Letters*, vol. 82, no. 26, pp. 4821-4823, 2003.

[16] G. Prakash, S. Hu, A. Raman and R. Reifenberger, "Theoretical basis of parametric-resonance-based atomic force microscopy", *Physical Review B*, vol. 79, pp. 094304-1-094304-10, 2009.

[17] G. Prakash, A. Raman, J. Rhoads and R. Reifenberger, "Parametric noise squeezing and parametric resonance of microcantilevers in air and liquid environments", *Review of Scientific Instruments*, vol. 83, pp. 065109-1-065109-12, 2012.

[18] M. Basso, P. Paoletti, B. Tiribilli and M. Vassalli, "Modelling and analysis of autonomous micro-cantilever oscillations", *Nanotechnology*, vol. 19, pp. 475501-1-475501-8, 2008.

[19] M. Basso, P. Paoletti, B. Tiribilli B and M. Vassalli, "AFM imaging via nonlinear control of self-driven cantilever oscillations"; *IEEE Transactions on Nanotechnology*, vol. 10, no. 3, pp. 560-565, 2011.

[20] K. L. Ekinci, M. H. Huang and M. L. Roukes, "Ultrasensitive nanoelectromechanical mass detection", *Applied Physics Letters*, vol. 84, no. 22, pp. 4469-4471, 2004.

[21] Y. T. Yang, C. Callegari, X. L. Feng, K. L. Ekinci and M. L. Roukes, "Zeptogram-scale nanomechanical mass sensing", *Nano Letters* vol. 6, no. 4, pp. 583-586 2006.

[22] A. K. Naik, M. S. Hanay, W. K. Hiebert, X. L. Feng and M. L. Roukes, "Towards single-molecule nanomechanical mass spectrometry", *Nature Nanotechnology*, vol. 4, pp. 445-450, 2009.

[23] S. Olcum, N. Cermak, S. C. Wasserman and S. R. Manalis, "High-speed multiple-mode mass-sensing resolves dynamic nanoscale mass distributions", *Nature Communications*, vol. 6, no. 7070, pp. 1-8, 2015.

[24] H. K. Lee, R. Melamud, S. Chandorkar, J. Salvia, S. Yoneoka and T. W. Kenny, "Stable operations of MEMS Oscillators far above the critical vibration amplitude in the nonlinear regime", *Journal of Micromechanical Systems*, vol. 20, no. 6, pp. 1228-1230, 2011.

[25] V. Zega, S. Nitzan, M. Li, C. H. Ahn, E. Ng, V. Hong, Y. Yang, T. Kenny, A. Corigliano and D. A. Horsley, "Predicting the closed-loop stability and oscillation amplitude of nonlinear parametrically amplified oscillators", *Applied Physics Letter*, vol. 106, pp. 233111-1-233111-5, 2015.

[26] W. J. Venstra, H. J. R. Westra and H. S. J. van der Zant, "Mechanical stiffening, bistability, and bit operations in a microcantilever", *Applied Physics Letters*, vol. 97, pp. 193107-1-193107-3, 2010.

[27] R. van Leeuwen, D. M. Karabacak, H. S. J. van der Zant and W. J. Venstra, "Nonlinear dynamics of a microelectromechanical oscillator with delayed feedback", *Physical Review B*, vol. 88, pp. 214301-1-214301-5, 2013.

[28] R. M. C. Mestrom, R. H. B. Fey and H. Nijmeijer, "Phase feedback for nonlinear MEM Resonators in oscillator circuits", *IEEE/ASME Transactions on Mechatronics*, vol. 14, no. 4, pp. 423-433, 2009.

[29] J. Mouro, B. Tiribilli and P. Paoletti, "Nonlinear behaviour of self-excited microcantilevers in viscous fluids", *Journal of Micromechanics and Microengineering*, vol. 27, pp. 095008-1-095008-12, 2017.

[30] J. Mouro, B. Tiribilli and P. Paoletti, "Measuring viscosity with nonlinear self-excited microcantilevers", *Applied Physics Letters*, vol. 111, pp. 144101-1-144101-4, 2017.

[31] Density of polystyrene beads: http://www.sigmaaldrich.com/catalog/product/sial/72986?lang=pt&region=PT (Last accessed: 07 December 2017)

[32] Density of glass beads: http://www.whitehousescientific.com/ekmps/shops/whisci/resources/Other/technical-specification-for-sodalime-glass.pdf (Last accessed: 07 December 2017)

[33] M. Bao, "Stress and strain of beam structures", in *Analysis and Design Principles of MEMS Devices*, 1st ed., Amsterdam, The Netherlands, Elsevier, 2005, pp. 46-63.

[34] J. L. Sader, "Frequency response of cantilever beams immersed in viscous fluids with applications to the atomic force microscope", *Jounal of Applied Physics*, vol. 84, no. 1, pp. 64-76, 2008.

[35] A. Maali, C. Hurth, R. Boisgard, C. Jai, T. Cohen-Bouhacina and J-P. Aimé, "Hydrodynamics of oscillating atomic force microscopy cantilevers in viscous fluids", *Journal of Applied Physics*, vol. 97, pp. 074907-1-074907-6, 2005.

[36] I. Dufour, A. Maali, Y. Amarouchene, C. Ayela, B. Caillard, A. Darwiche, M. Guirardel, H. Kellay, E. Lemaire, F. Mathieu, C. Pellet, D. Saya, M. Youssry, L. Nicu and A. Colin, "The microcantilever: a versatile tool for measuring the rheological properties of complex fluids", *Journal of Sensors*, vol. 2012, 719898, 2012.

[37] V. Kaajakari, T. Mattila, A. Oja and H. Seppa, "Nonlinear limits for single-crystal silicon microresonators", *Journal of Micromechanical Systems*, vol. 13, no. 5, pp. 715-724, 2004.

[38] Properties of the air: http://www.engineeringtoolbox.com/air-properties-d_156.html (Last accessed: 07 December 2017)

[39] S. Dohn, W. Svendsen, A. Boisen and O. Hansen, "Mass and position determination of attached particles on cantilever based mass sensors", *Review of Scientific Instruments*, vol. 78, pp. 103303-1-103303-3, 2007.

[40] G. Y. Chen, R. J. Warmack, T. Thundat, D. P. Allison and A. Huang, "Resonance response of scanning force microscopy cantilevers", *Review of Scientific Instruments*, vol. 65, no. 8, pp. 2532-2537, 1994.

[41] H. K. Khalil, "Frequency domain analysis of feedback systems", in *Nonlinear Systems*, 3rd ed., Upper Saddle River, NJ: Prentice-Hall, 2002, pp. 263-296.

[42] C. M. Jha, J. Salvia, S. A. Chandorkar, R. Melamud, E. Kuhl and T. W. Kenny, "Acceleration insensitive encapsulated silicon microresonator", *Applied Physics Letters*, vol. 93, pp. 234103-1-234103-3, 2008.

[43] I. Dufour, F. Josse, S. M. Heinrich, C. Lucat, C. Ayela, F. Ménil and O. Brand, "Unconventional uses of microcantilevers as chemical sensors in gas and liquid media", *Sensors and Actuators B*, vol. 170, pp. 115-121, 2012